Journal of Materials Science & Technology xxx (2020) xxx–xxx

Contents lists available at ScienceDirect

Journal of Materials Science & Technology

journal homepage: www.jmst.org

Invited Review

# Advanced Li-$Se_xS_y$ battery system: Electrodes and electrolytes

Huan Du [a], Shihao Feng [a], Wen Luo [a,b,*], Liang Zhou [a], Liqiang Mai [a,*]

[a] State Key Laboratory of Advanced Technology for Materials Synthesis and Processing, International School of Materials Science and Engineering, Wuhan University of Technology, Wuhan, 430070, China
[b] Department of Physics, School of Science, Wuhan University of Technology, Wuhan, 430070, China

ARTICLE INFO

*Article history:*
Available online xxx

*Keywords:*
Selenium–sulfur
Cathode materials
Electrolytes
Lithium–sulfur

ABSTRACT

The worldwide energy shortage has led to numerous researches for the exploration of new-type battery materials to deal with the energy crisis. To achieve a great leap in energy density, the study of high capacity electrode materials plays a major role. As a replacement to the energy accumulation system of lithium–sulfur (Li–S) and lithium–selenium (Li–Se) batteries, great concern is generated over lithium/selenium–sulfur (Li–$Se_xS_y$) batteries as they combine the advantages of S (high capacity) and Se (improved electrical conductivity), consequently stands for extensive new cathode materials. In recent years, widespread researches have been conducted and great achievements have been published. This review sums up the research status on Li–$Se_xS_y$ batteries and concentrates on the outstanding work of $Se_xS_y$ cathode materials. The reaction mechanism and capacity fading mechanism are discussed. The performance-structure relationship is stated in regard of different cathode structures, including a variety of carbon hosts, conducting polymer hosts, transition metal-doped carbon electrodes and various Se/S ratio. The compatibilities of frequently-used carbonate-based and ether-based electrolyte and other new-type electrolytes for Li-$Se_xS_y$ battery are demonstrated. Prospects for the future developments of Li–$Se_xS_y$ batteries are finally proposed.



,

**Contents**



* Corresponding authors at: State Key Laboratory of Advanced Technology for Materials Synthesis and Processing, International School of Materials Science and Engineering, Wuhan University of Technology, Wuhan, 430070, China.
*E-mail addresses:* luowen_1991@whut.edu.cn (W. Luo), mlq518@whut.edu.cn (L. Mai).

https://doi.org/10.1016/j.jmst.2020.01.001
1005-0302/

## 1. Introduction

For the past few years, rapid population growth and industrial production have put great pressure on natural resources, and thus raise concerns of sustainable energy because of the progressively increasing consumption of nonrenewable fossil fuels. Clean and renewable energy sources are in urgent required, which has promoted and accelerated the sustainable development of electricity supply systems [1–3]. For the last twenty years, lithium-ion batteries (LIBs) have made outstanding achievements in tiny-sized electronic devices. Nevertheless, the highest energy capacity that LIBs can deliver is far from enough for requirement even when fully developed [2,4–8]. Electric vehicles, for instance, require high gravimetric and volumetric energy density simultaneously.

Gradually, more researchers discover that Li–S and lithium–oxygen ($Li–O_2$) batteries are superior and demonstrate much higher energy density than traditional LIBs. Unfortunately, $Li–O_2$ batteries are confronted with a series of problems, including poor cycling performance, unstable electrolyte and large voltage polarization [9,10]. Li–S battery is a better choice and closer to practical realization which have been under research for several years. Sulfur cathode is more suitable owing to its lower price, abundance, nontoxicity and higher specific capacity. However, in the meantime, Li–S batteries also suffer from limited rate performance, capacity fading problem and shuttle effect, which is a phenomenon of cyclic migration of the intermediates between cathode and anode. These deficiencies can be attributed to the dissolution of intermediate polysulfides and low conductivity of S [2,11–14].

Selenium (Se), $[Ar]4s^2 3d^{10} 4p^4$, has been investigated and applied as new electrode materials for renewable batteries in recent years [15]. Li–Se batteries show better rate and cycling performance benefited from the high conductivity of Se ($1 \times 10^{-3}$ S m$^{-1}$), compared with S ($5 \times 10^{-28}$ S m$^{-1}$). Meanwhile, Li–Se batteries not only possess a higher theoretical volumetric capacity (3253 mA h cm$^{-3}$), but also deliver a higher output voltage. All these advantages make Se potential electrode materials for lithium storage. Unfortunately, Li–Se batteries are also limited because of the inferior gravimetric capacity (675 mA h g$^{-1}$), less abundance of Se in earth, undesirable cost and are also faced with problems of shuttle effect and capacity fading [16–19].

A new battery concept, $Li–Se_xS_y$ battery, has been invented by researchers in Argonne National Lab in 2012, indicating the suitability of $Se_xS_y$ as cathodes for rechargeable lithium batteries as well as sodium batteries [20]. They have noticed higher energy density than Se and superior reaction kinetics and conductivity compared to S were shown during cycling when using $SeS_2$ as an electrode. Since then, $Se_xS_y$ cathodes have been brought into focus and a wide variety of $Se_xS_y$–carbon cathode materials have been fabricated for lithium energy storage system.

However, research on $Li–Se_xS_y$ batteries is still in its infancy and fundamental issues still exist. Due to the limited surface areas and pore volumes of carbon hosts, $Li–Se_xS_y$ batteries face the issue of dissolution and shuttling of $Se_n^{2-}/S_n^{2-}$ in electrolyte [21]. Second, due to density differences between $Se_xS_y$ (3 g cm$^{-3}$ for $SeS_2$) and $Li_2Se$ (2.86 g cm$^{-3}$) /$Li_2S$ (1.67 g cm$^{-3}$), $Se_xS_y$ experiences large volume expansion during lithiation, which the volume expansion ratio of $SeS_2$ can be as high as 83.4%. As a result, the potential of the $Se_xS_y$-based cathode materials has not been fully confirmed in the initial research stage.

Recently, many strategies have been conducted in order to facilitate the electrochemical properties of $Se_xS_y$ electrodes. To address the issues of low conductivity and shuttle effect, carbon host materials with higher specific surface areas and improved electrical conductivity have been utilized to encapsulate the $Se_xS_y$ molecules. Thus, it is essential to design electrodes rationally with hierarchy on structural, morphological and porous component levels through introducing conductive component for better practical applicability. The design of hierarchically nanostructured electrodes for $Li–Se_xS_y$ batteries can significantly facilitate the stability and conductivity of electrode composite, and also improve the electrochemical performance to a great extent. After the introduction of $Se_xS_y$ materials, many studies exploring the optimal Se/ S ratio have been carried out and discussed to gain the superior capability at cheap price [22]. The optimization on the ratio of $x/y$ in $Se_xS_y$ materials plays an important role in electrochemical performance as $Se_xS_y$ cathodes with different Se/S ratios have distinct electrochemical behaviors. For instance, the higher S content in the composites, the higher discharge capacity will be achieved because of the contribution of S to the overall capacity.

As is known to all, the organic electrolytes make a difference on the performance for LIBs [23]. When changing the different composition of the electrolyte in Li–S batteries, for instance, the cycle life could be greatly lengthened [24]. Similarly, $Li–Se_xS_y$ battery system also highly relies on the nature of the electrolytes. Carbonate-based electrolyte and ether-based electrolyte are most applied in subsequent research generally, in which $Se_xS_y$-based electrode has been proven that it can work in both of them but each has its advantages and disadvantages [18]. New-type electrolytes including all-solid-state electrolyte and solid/liquid hybrid electrolyte have also been proposed [25].

This paper systematically reviews the research status of $Li–Se_xS_y$ batteries and mainly concentrates on the recent research progress of the design and synthesis of micro/nanostructured electrodes. The performance-structure relationship is stated in regard of different cathode structures, including mesoporous/microporous carbon hosts, hollow carbon hosts, carbon nanofiber/carbon nanotube-based hosts, conducting polymer hosts, transition metal-doped carbon hosts and various Se/S ratios. In addition, the reaction mechanism of $Li–Se_xS_y$ batteries and the comparison of different electrolytes are discussed intensively, which would indicate the direction on the future development of $Li–Se_xS_y$ batteries (Fig. 1).

## 2. Reaction mechanism of $Li–Se_xS_y$ batteries

### 2.1. (De)lithiation mechanism

The charge–discharge process of $Li–Se_xS_y$ batteries is relatively complicated, which the reaction mechanism shows obvious difference between carbonate-based electrolytes and ether-based electrolytes, which results from different solubility of the redox products in different electrolytes [26].

In ether-based electrolytes, Se and S cathodes experience a similar two-step lithiation process. Cui et al. used high-energy X-ray diff

Please cite this article in press as: H. Du, et al., J. Mater. Sci. Technol. (2020), https://doi.org/10.1016/j.jmst.2020.01.001

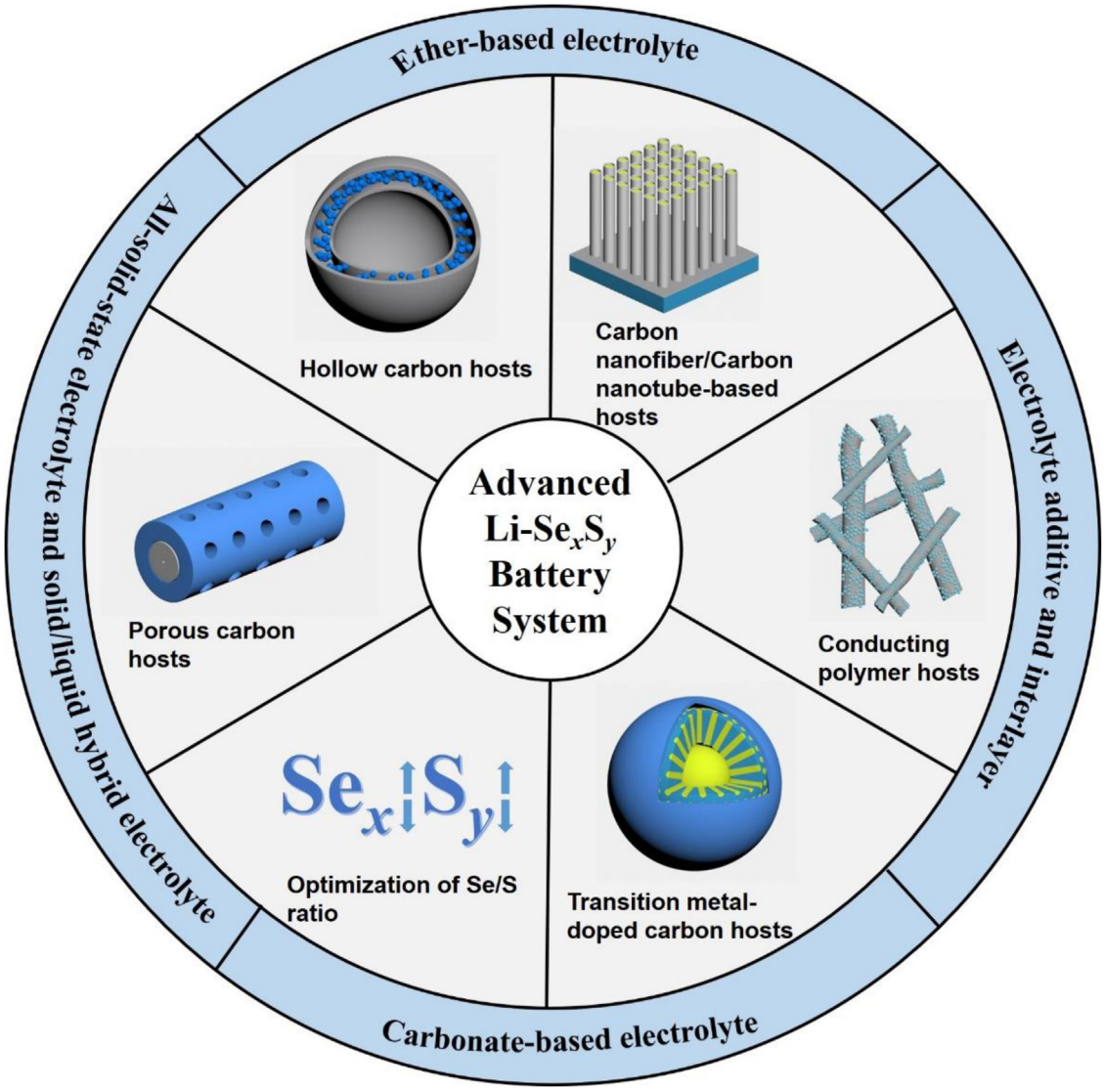


**Fig. 1.** Schematic of different hosts and electrolytes as optimization strategies for Li–Se$_x$S$_y$ batteries.

;raction (HEXRD) and X-ray absorption spectroscopy (XAS) analysis to investigate the (de)lithiation mechanism of Li–SeS$_x$ batteries [27]. As shown in Fig. 2(a), in the discharge process, Se was firstly reduced to $Li_2Se_n$ ($n \geq 4$), and the corresponding discharge voltage platform was 2.04 V. After that, $Li_2Se_n$ was reduced to $Li_2Se_2$ and $Li_2Se$, and the corresponding discharge voltage platform was 1.95 V. When charging, $Li_2Se$ was straight oxidized to $Li_2Se_n$ and oxidized to Se later. It was believed the oxidation peak stood for the processes of $Li_2Se$ to $Li_2Se_n$ and then to Se. They also verified the existence of polyselenides in ether-based electrolyte, which exhibited more soluble than both Se and $Li_2Se$ [28].

To further comprehend the (de)lithiation mechanism in ether-based electrolytes, the schematic discharge reaction model of the $SeS_2$@mesoporous carbon aerogels (MCA) composite cathode was put forward in the report of Zhang's group, which can be concluded as a four-step reduction reaction during discharge process as shown in Fig. 2(b) [29]. The first and third steps correspond to the transformation of high-order polysulfides to low-order polysulfides and then to $Li_2S_2$ and $Li_2S$, while the second and fourth steps stand for the transformation of Se to polyselenides and then to $Li_2Se$.

In carbonate-based electrolytes, an obvious plateau near 2 V during discharge process is observed, which corresponds to one single process: Se is reduced into $Li_2Se$ directly in Li–Se batteries without the existence of intermediate phases (Fig. 2(c)). This can be explained that the redox products, including Se, $Li_2Se$ and $Li_2Se_n$, are insoluble in the electrolyte. Cui et al. used X-ray absorption near edge structure (XANES) spectroscopy to confirm this discovery and the fitting results also revealed that no obvious intermediate phases and lithium polyselenides were formed in the carbonate-based electrolyte, which can efficiently enhance the cycling performance without the influence of intermediate phases [26].

### 2.2. Capacity fading mechanism

Even with a well encapsulation of Se$_x$S$_y$ in various carbon host materials, it was found that the majority of the cathodes still demonstrated an obvious capacity decay in ether-based electrolytes [30–35]. Xu and co-workers developed $Se_2S_5$ as cathode materials, which displayed a rapid capacity fading during cycling as mentioned [36]. The battery demonstrated a well-performed initial capacity of 1564.6 mA h g$^{-1}$, however, it just maintained 345.5 mA h g$^{-1}$ after 50 cycles (Fig. 2(d)). Likewise, similar capacity decay phenomena also appeared in previously reported articles when using ether-based electrolytes. By contrast with Se/microporous carbon (MPC) composite whose cycling performance showed a significant capacity decay as well, they concluded that Se components in the

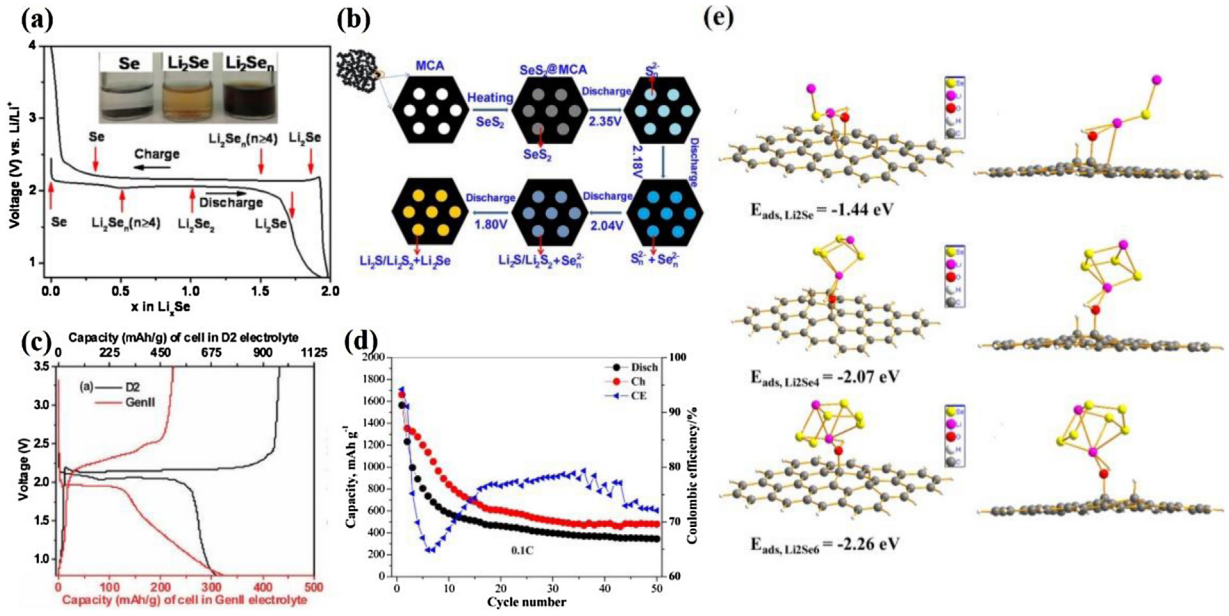


**Fig. 2.** (a) Mechanism of cathode phase transfer of Li–Se batteries in ether-based electrolytes [27]. (b) Schematic model of discharge reaction of $SeS_2$@MCA cathode [29]. (c) Voltage curves of Li–Se battery in carbonate-based (GenII) and ether-based (D2) electrolytes [26]. (d) Cycling performance of $Se_2S_5$/MPC cathode at 0.1 C and (e) the binding energy of diff ;erent polyselenides with carbon matrixes [36].

composites resulted in the rapid capacity decay of the $Se_2S_5$/MPC composite [37].

To reveal the mechanism of capacity fading, they conducted ab initio calculations to calculate the value of surface interaction [36]. They discovered that there was a bonding preference of long chain polyselenides with carbon surface, according to the order of $Li_2Se_6$> $Li_2Se_4$> $Li_2Se$, as shown in Fig. 2(e). Since shorter-strand polyselenides behaved harder to bond with carbon surface, the conversion of long-strand polyselenides to short-strand polyselenides was restrained in the charge–discharge process. Therefore, the amount of long-strand polyselenides may be intensified while working. Furthermore, these redundant polyselenides could diff ;use to and react with the Li anode, forming short-strand polyselenides, then oxidized to long-strand polyselenides again while charging. This vicious circle result in shuttle phenomenon and severe corrosion of Li anode, and eventually leads to the unsatisfactory Coulombic efficiency and fast capacity fading [38].

## 3. Optimization of $Se_xS_y$ cathodes

As discussed above, Li–$Se_xS_y$ batteries suffer from volume expansion, low conductivity and shuttle effect. To address these problems, the most typical method is to develop different forms of carbonaceous electrode by using nano-sized carbon materials to be host materials according to the similar method in Li–Se batteries [39–43]. Furthermore, shuttle effect can be efficiently inhibited due to the absorption force of $Se_xS_y$ molecules with the carbon matrix and the conductivity of $Se_xS_y$ can be significantly improved. As shown in Table 1, carbonaceous materials have been fabricated and applied as electrode materials for Li–$Se_xS_y$ batteries most widely and extensively.

It is reported that the optimization methods of $Se_xS_y$ cathodes can be summed as two main aspects, including selection of different carbon hosts and adjusting the Se/S ratio. A variety of carbon forms are reviewed, consisting of porous, hollow, nanofiber, nanotube, conducting polymer and transition metal-doped carbon hosts. The optimal Se/S ratio also results in superior electrochemical performance and better application potential in Li–$Se_xS_y$ batteries. The optimization of carbon hosts and Se/S ratio will be discussed in the following parts.

### 3.1. Porous carbon hosts

Among all aforementioned materials, porous carbon materials have been viewed as the most employed and lucubrated hosts and received the widest recognition. The porous carbon host can act as a shield to prevent the mass loss of active material when $Se_xS_y$ molecules are infiltrated into porous carbon, improve electrical conductivity and also reduce the $Li^+$ diffusion length benefited from continuous carbon networks [44,45]. Besides, pores with different morphologies and architectures acquire different efficacy of the properties of Li–$Se_xS_y$ batteries. Undersized pores (micropores) in porous carbon hosts have an effect of containing active materials for a more stable cycling performance, for instance, while large-sized pores (mesopores) act as a role of channels for electrolyte for enhanced rate property of Li–$Se_xS_y$ batteries [46].

#### 3.1.1. Microporous carbon hosts

Microporous carbon materials with various architectures have been extensively synthesized as suitable $Se_xS_y$ hosts because of their high specific surface areas, large adsorption volumes and porosity structures for $Se_xS_y$ impregnation. Specifically, benefited from volume constraints, the microporous carbon materials with undersized pores (<2 nm) can efficiently prevent the polyselenides from dissolution [47]. Xin et al. fabricated conductive microporous carbon matrix to confine metastable small sulfur molecules of $S_{2-4}$ for Li–S batteries [48]. The use of microporous carbon host can prevent the large $S_8$ from forming soluble polysulfides, and thus the shuttle effect can be totally avoided. Liu et al. developed a novel Se–carbon cathode through infusing Se in a microporous carbon polyhedron (Se@MICP) for Li–Se batteries, thus effectively encapsulated Se and suppressed the dissolution of polyselenides to electrolyte. However, the use of microporous carbon host in the field of Li–$Se_xS_y$ batteries is not common and needs further development [49].

Xu's group developed a $Se_2S_5$/microporous carbon (MPC) cathode through a synthesis process of modified

**Table 1**
Summary of representative Li–$Se_xS_y$ batteries.

| Cathode material | Initial capacity (mA h $g^{-1}$) | Capacity retention (mA h $g^{-1}$) | CycleNo. | Rate | Coulombic efficiency | Electrolyte | Ref. |
|---|---|---|---|---|---|---|---|
| C-$SeS_2$ | ~450 | 512 | 30 | 50 mA $g^{-1}$ | – | 1.2 M $LiPF_6$/EC–DMC | [20] |
| $Se_2S_5$/MPC | 1661.2 | 345.5 | 50 | 0.1 C | 94.1% | 1 M LITFSI in DOL/DME+0.1 M $LiNO_3$ | [36] |
| CMK-3/$SeS_2$@PDA | 800 | 350 | 500 | 2 A $g^{-1}$ | ~100% | 1 M LiTFSI in DOL/DME+0.2 M $LiNO_3$ | [51] |
| $Se_2S_5$/MCM | 1150.6 | 610 | 100 | 0.5 C | ~100% | 1 M LITFSI in DOL/DME | [22] |
| $SeS_2$@MCA | 846 | 308 | 130 | 500 mA $g^{-1}$ | – | 1 M LITFSI in DOL/DME+0.1 M $LiNO_3$ | [29] |
| $Se_2S_6$/NMCs | ~1200 | 780 | 200 | 250 mA $g^{-1}$ | 96.5% | 1 M LITFSI in DOL/DME | [58] |
| $SeS_2$/HCS | 956 | 235.1 | 200 | 100 mA $g^{-1}$ | 95.8% | 1 M LiPF6/EC + DEC | [64] |
| $SeS_2$/DLHC | 990 | 930 | 100 | 200 mA $g^{-1}$ | ~100% | 1 M $LiPF_6$/EC–DEC–DMC | [65] |
| $S_{0.6}Se_{0.4}$@CNFs | ~500 | 346 | 1000 | 1A $g^{-1}$ | ~100% | 1 M $LiPF_6$/EC–DEC | [69] |
| $S_{1-x}Se_x$/CNFs | ~1050 | ~600 | 50 | 0.05 C | >98% | 1 M LITFSI in DOL/DME+0.2 M LiNO3 | [72] |
| MWCNTS-$SeS_2$ | ~1400 | 571 | 50 | 50 mA $g^{-1}$ | ~100% | 1.0 M LiTFSI in DOL/DME | [27] |
| $Se_xS_{8-x}$-M32/VACNTs | 1031 | ~800 | 500 | 500 mA $g^{-1}$ | 93% | 1.0 M LiTFSI +0.1 M $LiNO_3$ in DOL/DME | [77] |
| pPAN/$SeS_2$ | 871 | 633 | 2000 | 4 A $g^{-1}$ | – | 1 M $LiPF_6$/EC–DEC | [84] |
| CPAN/$SeS_2$ | ~800 | 780 | 1200 | 600 mA $g^{-1}$ | ~100% | 1 M $LiPF_6$/EC–DEC | [89] |
| CO-N-C/$SeS_2$ | 1165.1 | 970.2 | 200 | 0.2 C | ~100% | 1 M LITFSI in DOL/DME | [94] |
| $NiCo_2S_4$@NC–$SeS_2$ | 678.6 | 557 | 800 | 1 C | 98% | 1.0 M LiTFSI +0.1 M $LiNO_3$ in DOL/DME | [95] |
| $CoS_2$@LRC/$SeS_2$ | 868 | 470 | 400 | 0.5 A $g^{-1}$ | 97% | 1 M LITFSI in DOL/DME+0.1 M $LiNO_3$ | [102] |
| HMC@TiN/ $SeS_2$ | 987 | 690 | 200 | 0.2 C | ~99% | 1 M LITFSI in DOL/DME+0.2 M $LiNO_3$ | [104] |
| $SeS_2$–LPS–C | 889 | 782 | 50 | 50 mA $g^{-1}$ | ~100% | All-solid-state electrolytes | [25] |

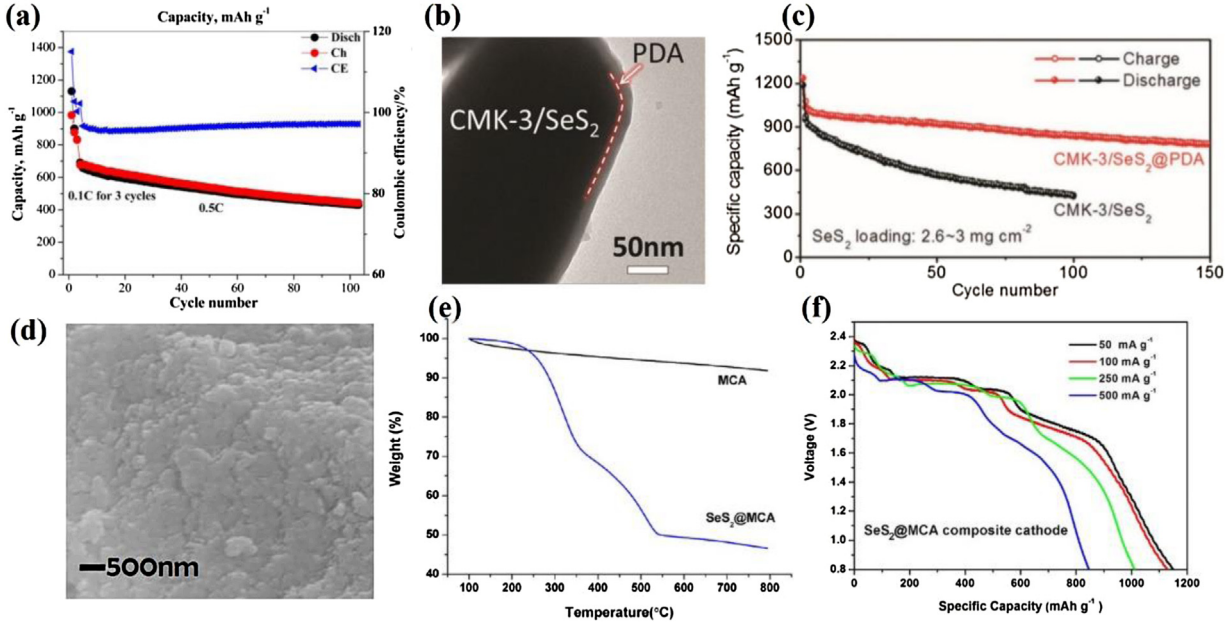


**Fig. 3.** (a) Cycling performance of $Se_2S_5$/MPC cathode at 0.5 C [36]. (b) TEM image of CMK-3/$SeS_2$@PDA and (c) cycling performance of CMK-3/$SeS_2$@PDA cathode at 0.2 A $g^{-1}$ [52]. (d) SEM image of $SeS_2$@MCA, (e) TGA curves of MCA and $SeS_2$@MCA composites and (f) the discharge profile of $SeS_2$@MCA cathode in the first cycle [29].

vaporization–condensation to investigate the reaction process, which revealed the gradual reduction of the lithiation and delithiation reversibility during cycling [36]. This caused the generation of long-strand polyselenides considerably and capacity loss, as mentioned above. As for electrochemical properties, when the battery was firstly cycled at 0.1 C for 3 cycles and then cycled at 0.5 C for the following cycles instead of continuous cycling at 0.1 C, as exhibited in Fig. 3(a), the $Se_2S_5$/MPC delivered an initial discharge capacity of 691.9 mA h $g^{-1}$ and still displayed a stable capacity (430.2 mA h $g^{-1}$) after 100 cycles, demonstrating efficiently avoidance of capacity fading and better reversible capacity.

### 3.1.2. Mesoporous carbon hosts

The mesoporous carbon materials, with high specific surface area, appropriate pore size distribution (2–50 nm), have many advantages such as outstanding confinement capabilities for polysulfides and polyselenides, large contact areas with active material, and superior conductivity [50]. After developing a set of mesoporous hosts with different pore sizes for Li–S batteries, Li et al. reported that large-sized mesoporous carbon hosts could confine sulfur molecules more efficiently and keep a relatively superior electrochemical performance even when sulfur is located full of the pore areas [51].

Lou and his co-workers confined $SeS_2$ within a highly ordered mesoporous carbon (CMK-3) framework and used polydopamine (PDA) as a shelter to synthesize an advanced and high $SeS_2$ mass loading cathode for Li–$SeS_2$ batteries [52]. Through confinement, the highly ordered carbon channels could be detected, providing electrochemical reaction chambers on a nanometer-scale and making active materials have sufficient contact with electrons, thus making it easy to redox react faster (Fig. 3(b)). Meanwhile, the external PDA shelter played the role of a barrier to prevent redox intermediates from being insoluble, hence increasing the availability of active material and stabilizing the cycle life. The CMK-3/$SeS_2$@PDA cathode delivered a high capacity of over 1200 mA h

$g^{-1}$ at 0.2 A $g^{-1}$ and maintained over 500 cycles at 2 A $g^{-1}$ as illustrated in Fig. 3(c).

Benefited from appropriate pore sizes and large surface areas, mesoporous carbon spheres also have been fabricated for $Se_xS_y$ hosts, which can absorb the polysulfides and polyselenides efficiently and keep them stay inside of mesopores, thereby imposing restrictions on needless electrochemical reactions between $Li^+$ and active material [53]. Wei et al. adopted a spray-drying assisted hard template method to develop mesoporous carbon microsphere (MCM) hosts for Li–$Se_2S_5$ batteries [22]. In the electrochemical test, $Se_2S_5$/MCM cathode exhibited outstanding rate property (688.8 mA h $g^{-1}$ at 5 C), delivered a high reversible capacity of 796.4 mA h $g^{-1}$ at 0.5 C and maintained over 100 cycles. Particularly, a perfect Coulombic efficiency reached nearly 100% without adding $LiNO_3$. The anchor effect of Se–S bonds in $Se_2S_5$/MCM composites can efficiently avoid forming and dissolving long-chain intermediates [54].

Three-dimensional (3D) mesoporous carbon aerogels (MCA) are promising and advanced host materials with highly porous and small particles. Benefited from their high electrochemical conductivity, high porosity and surface areas, controllable pore structures, they have attracted more attention and proven to be suitable for rechargeable batteries [55–57]. Herein, Zhang et al. adopted melt-back diffusion method to confine $SeS_2$ in MCA to synthesize $SeS_2$@MCA cathode material [29]. As shown in Fig. 3(d), field emission scanning electron microscopy (FESEM) image of $SeS_2$@MCA composite obviously revealed that porous structure still existed after the encapsulation of $SeS_2$. Besides, the weight content of $SeS_2$ was tested to be 49.3 wt% via thermogravimetric (TG) analysis (Fig. 3(e)). The $SeS_2$@MCA delivered an initial discharge capacity of 1150 mA h $g^{-1}$ and 601 mA h $g^{-1}$ for the ensuing 10 cycles (Fig. 3(f)). The electrochemical performance is superior than pristine $SeS_2$ cathode, which can be explained by the polysulfides and polyselenides effectively trapped through the porous structure of the MCA.

Sun et al. reported that the existence of weak interactions between the $Se_xS_y$ materials and the carbon conductive hosts would lead to inevitable shuttle phenomenon. Fortunately, this can be avoided by enhancing and strengthening the interactions between $Se_xS_y$ molecules and carbon host materials in the electrolyte [58]. Based on this, they fabricated $Se_nS_{8-n}$/N-doped carbon mesoporous carbons (NMCS) by encapsulating heteroatomic $Se_nS_{8-n}$ materials into nitrogen-doped mesoporous carbons (NMCs) through a simple melt impregnation process, as the nitrogen doping can benefit the formation of selenium bonds to mitigate the polyselenides shuttling (Fig. 4(a)). As illustrated in Fig. 4(b), a high reversible capacity maintained 780 mA h $g^{-1}$. Besides, they conducted density functional theory (DFT) calculations, which revealed that $Se_xS_y$ molecules with higher polarizability tended to have a stronger bind with NMCs and provide more efficient suppression of the shuttle effect than homoatomic sulfur molecules.

### 3.2. Hollow carbon hosts

Among all porous carbon materials, hollow carbon spheres (HCSs) are particularly attractive for S or $Se_xS_y$ loading. The large cavity and porous shell, in principle, allow for more active material loading than other porous carbon materials; meanwhile, the porous shell, which operates as a physical barrier could restrain the dissolution and shuttling of $Se_n^{2-}$/$S_n^{2-}$ [59].

High porosity nanostructured hollow carbon spheres have been researched and developed to immobilize a large number of active material components, such as sulfur. The results show that sulfur is more likely to accumulate in the highly porous carbon shells than in the inner cavity or interlaminar void of the multi-shelled hollow hosts [60–63]. Luo et al. adopted the melt-back diffusion method for fabricating a $SeS_2$-impregnated hollow carbon sphere (HCS) composite. It delivered an initial discharge capacity of 956 mA h $g^{-1}$ in the first cycle at 100 mA $g^{-1}$ and exhibited a long cycle life of 200 cycles [64].

Yu's group also fabricated $SeS_2$/double-layered hollow carbon spheres (DLHC) cathode via a hot-melt impregnation technique as shown in Fig. 4(c) [65]. $SeS_2$/DLHC cathode delivered 930 mA h $g^{-1}$ at 0.2 C and exhibited superior rate property of 400 mA h $g^{-1}$ at 6 C. As illustrated in Fig. 4(d), the $SeS_2$/DLHC battery displayed 11% capacity fading over 900 cycles and only 0.012% capacity fading each cycle, indicating an ultra-long cycle life. The superior performance can be explained by the following three reasons: firstly, a large amount of areas for the location of $SeS_2$ to rise its loading ratio owing to the interlayer void and a buffer space for the large volume variations of $SeS_2$ owing to hollow cavity; secondly, the efficiently suppression of shuttling phenomenon of polysulfides owing to microporous carbon shells; thirdly, the highly enhanced conductivity of electrodes owing to Se component and carbon skeleton.

### 3.3. Carbon nanofiber/Carbon nanotube-based hosts

Carbon nanofibers (CNFs) attract much attention due to their high conductivity and strength. On one hand, the high electron conductivity makes CNFs become suitable conductors. On the other hand, the CNFs could build an interconnected porous network with high porosity for promoting electrolyte infiltration and buffering volume changes during the charge and discharge. Besides, the introduction of CNFs can lessen contact between $Se_xS_y$ and the CNFs matrix and alleviate the dissolution of active material [66–68].

Yao et al. fabricated a flexible $S_{0.6}Se_{0.4}$@CNFs cathode and exhibited outstanding cycle and rate performance via a one-step synthesis procedure, which was prepared by co-heating $S_{0.6}Se_{0.4}$ and polyacrylonitrile (PAN) nanofibers as shown in Fig. 5(a) and (b) [69]. It is worth noting that the battery demonstrated an ultra-long cycle life, which maintained a capacity of 346 mA h $g^{-1}$ for over 1000 cycles (Fig. 5(c)). CNFs have effects of acting as infiltration pathways for electrolyte, promoting electrons transfer, and shortening the ion diffusion length [70]. In addition, benefited from constructing C–S bond, the core/shell structure brings the effects of physical confinement and chemical binding. The two effects synergistically result in better availability of cathode materials by retarding the dissolution of intermediates in electrolyte [71]. Pandey et al. also fabricated $S_{1-x}Se_x$/CNFs material for improved Li–$Se_xS_y$ batteries [72]. The $S_{1-x}Se_x$/CNFs electrode delivered a good capacity of nearly 1050 mA h $g^{-1}$ at 0.05 C and exhibited high mass loading.

Multi-walled carbon nanotubes (MWCNTs) are common carbon hosts based on $sp^2$ hybridized carbon, which can improve the electrical conductivity and the electrochemical performance of the cathode. Nevertheless, the utilization of active material is not high enough and they still experience fast capacity fading when active material is mixed with CNTs, which can be explained by the poor contact between C and $Se_xS_y$ [66,73]. By functionalizing the surface of CNTs, the intermediates can be efficiently anchored through the chemical bonding between $Se_xS_y$ molecules and functional groups. Amine's group prepared $SeS_x$/MWCNTs composites via a solution-based and melt-infusion process and $SeS_2$/MWCNTs achieved a balance among efficiency, capacity and retention [27]. The Li–$SeS_2$ battery maintained a discharge capacity of over 571 mA h $g^{-1}$ after 50 cycles with a second discharge capacity of 0.9 mA h $cm^{-2}$.

Benefited from its superior physical properties, 3D array structure is also suitable when it comes to the design of CNTs structure, including abundant hollow spaces to improve electrolyte infiltration and the interactions of active materials with nanoarray

Please cite this article in press as: H. Du, et al., J. Mater. Sci. Technol. (2020), https://doi.org/10.1016/j.jmst.2020.01.001

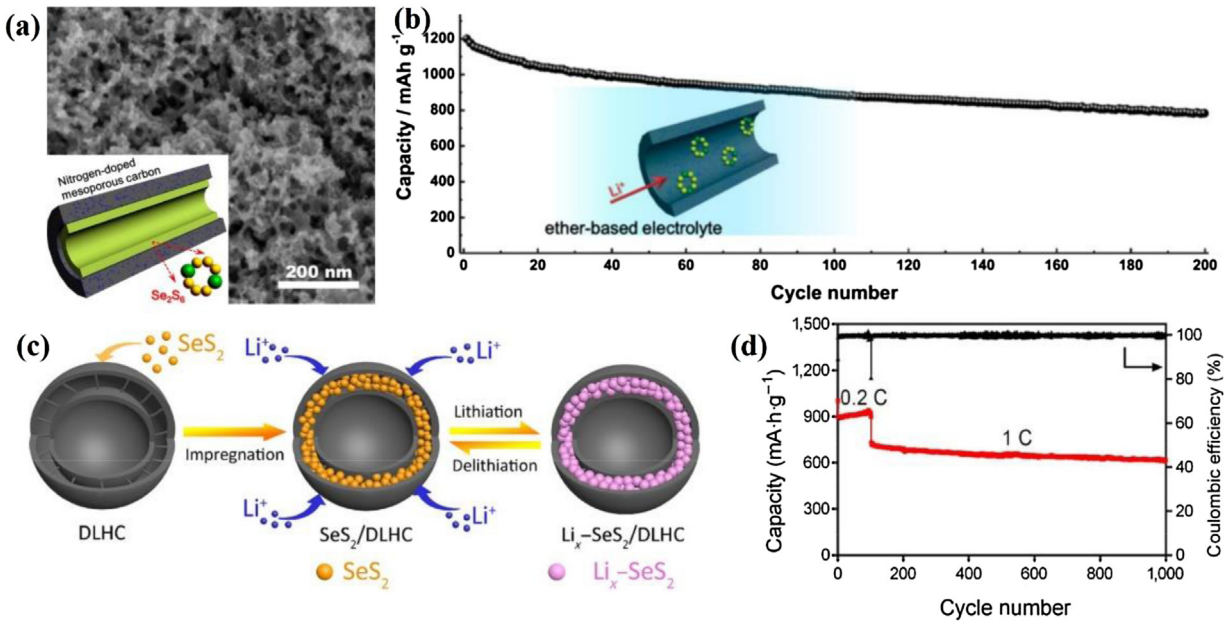


**Fig. 4.** (a) SEM image of $Se_2S_6$/NMC and schematic model of the $Se_2S_6$/NMC internal structure and (b) cycling performance of $Se_2S_6$/NMC at 250 mA $g^{-1}$ [58]. (c) Schematic fabrication model of DLHC spheres and (d) cycling performance of $SeS_2$/DLHC [65].

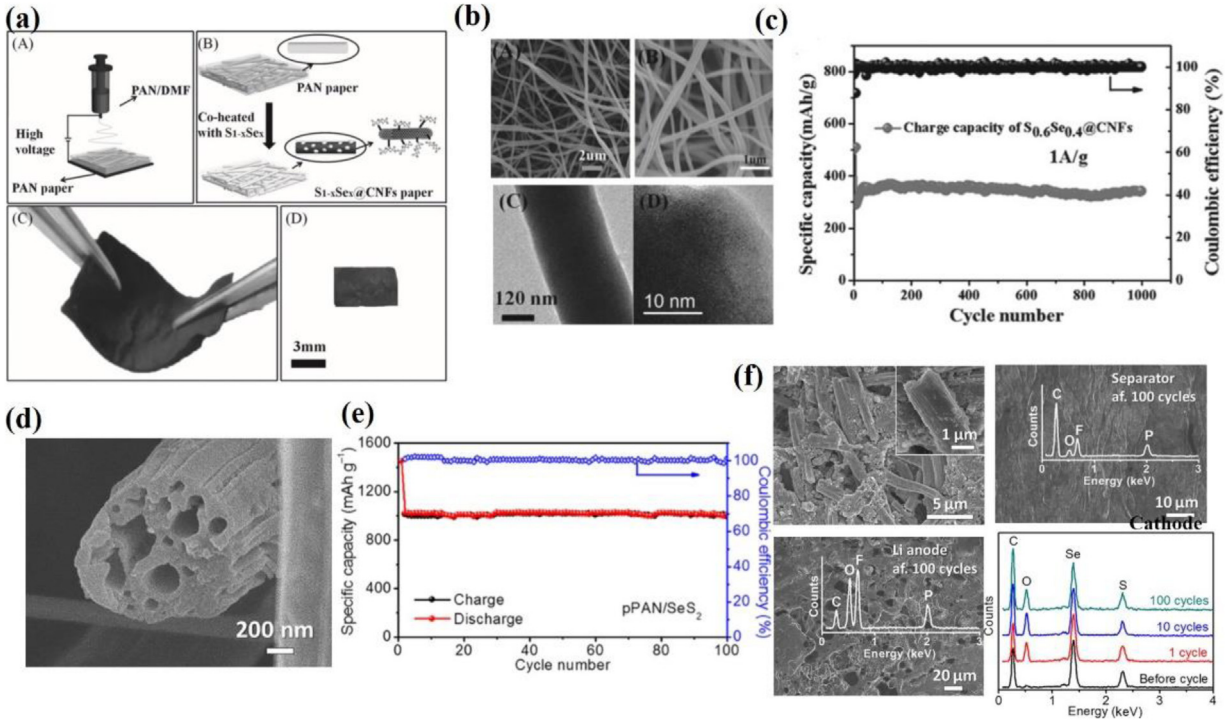


**Fig. 5.** (a) Schematic synthesis model and photograph of $S_{1-x}Se_x$@CNFs composite, (b) SEM images of PAN (A) and $S_{0.6}Se_{0.4}$@CNFs (B), TEM (C) and HRTEM (D) images of $S_{0.6}Se_{0.4}$@ CNFs and (c) cycling performance of $S_{0.6}Se_{0.4}$@CNFs at 1 A $g^{-1}$ [69]. (d) SEM image of pPAN/$SeS_2$, (e) cycling performance of pPAN/$SeS_2$ battery at 0.5 A $g^{-1}$ and (f) SEM images of 100 times cycled pPAN/$SeS_2$ electrode films and separator and Li anode. Insets are EDX curves of separator, Li anode and cathode films, respectively [84].

skeleton for higher reaction stability [74–76]. Fan et al. fabricated boron- and nitrogen-doped vertically aligned CNTs (VACNT) for the confinement of $Se_xS_{8-x}$ [77]. On one hand, the CNTs permitted fast electron migration for high rate performance and high active material utilization. On the other hand, the vertically aligned structure offered unidirectional void sites to avoid volume changes and shuttle phenomenon of polysulfides and polyselenides. Moreover, the B- and N-doped graphene layers were bonded by COOH- and OH-enriched polyacrylic acid binder, which effectively immobilized active materials inside of the CNTs when cycling. In the meantime, the cathode demonstrated an outstanding capacity at 0.5 A $g^{-1}$ after 500 cycles (818 mA h $g^{-1}$).

### 3.4. Conducting polymer hosts

Conducting polymers, such as polyaniline, polypyrrole and polyacrylonitrile, benefited from their functional groups, peculiar chain structures and superior conductivity, have been synthesized to

confine active materials and decrease the polyselenides and polysulfides in electrodes [30,78,79]. In addition, the soft and flexible conducting polymer can be used to solve volume changes and electrode collapse during cycling and facilitate the electrochemical performance. On one hand, the volume changes would not easily break the external protective layer owing to the flexible polymer host. More importantly, the capacious internal structure of the polymer host is suitable for Li diffusion to reach the interior $Se_xS_y$ materials.

In Li–S batteries, compared with porous carbon materials, which are complicated generated, polyacrylonitrile (PAN) attracts more attention for simple fabrication. Because it is easy to dehydrogenate and cyclize into conjugated skeletons, the pyrolyzed PAN (pPAN)/S cathode can be developed via a simple one-step reaction [80,81] and reaction mechanisms have been successfully revealed [82,83]. Lou and co-workers designed and synthesized a pPAN/$SeS_2$ composite by aforementioned heating method, which made active material content reach 63 wt% as shown in Fig. 5(d) [84]. The pPAN/$SeS_2$ cathode exhibited superior electrochemical performance. In Fig. 5(e), the pPAN/$SeS_2$ cathode delivered a high initial capacity of 1451 mA h $g^{-1}$ when cycled at 0.5 A $g^{-1}$, and then stabilized at about 1020 mA h $g^{-1}$ in the ensuing cycles. Previous research reported that the existence of short $S_x$ chains, which covalently bonded to the cyclized PAN skeletons via C—S bonds [40,85]. Therefore, it is reasonable that there might be short $Se_xS_y$ chains covalently bonded to PAN skeletons, with Se presented in every short chain, which will effectively improve the activity of the cathode material owing to the outstanding reaction kinetics of Se component. And more notably, no Se or S appeared on the surfaces of the separator and the Li metal anode, indicating completely avoidance of dissolution of polysulfides and polyselenides in pPAN/$SeS_2$ composites (Fig. 5(f)).

Previous research reported the reaction between PAN and sulfur at a temperature of 300 °C and the heterocyclic products are stable and conductive, which can stabilize sulfur and polysulfides [86,87]. After continued rising the temperature to 600 °C, the N-containing structures in carbonized PAN(CPAN) possess the ability of restricting lithium polysulfides, hence improving the cycling stability and electron conductivity [88]. Wang's group fabricated $SeS_{0.7}$/CPAN composites through simple annealing method [89]. The dissolution of polysulfides and polyselenides in carbonate-based electrolyte was effectively decreased and the cycling stability of $SeS_x$/CPAN battery was greatly enhanced due to the confinement of $SeS_x$ materials by N-containing carbon circular structures in CPAN. The cell delivered a relatively good capacity (780 mA h $g^{-1}$), demonstrated a very long cycle life (1200 cycles) and superior rate property from 60 mA $g^{-1}$ to 6 A $g^{-1}$. Particularly, solid electrolyte interphase (SEI) film was detected on the cathode surface in the initial cycle, which further prevented polysulfides and polyselenides from dissolution and avoided reaction between cathode and carbonate-based electrolyte.

### 3.5. Transition metal-doped carbon hosts

Heteroatom doping is commonly used as electrode materials for LIBs, which can assist to form the carbon functional group–selenium bonds to decrease the shuttle effect and form a flatter plateau and lower overpotentials [90]. Through heteroatom doping, the electrical conductivity of carbon hosts can be enhanced, the reaction active sites get increased, and the accessibility and absorption of the electrolyte can be promoted [91]. Therefore, the heteroatom-doped carbon hosts could further facilitate the electrochemical properties of Li–$Se_xS_y$ batteries.

For example, Li and Yin used microporous carbon layers to fabricate N-doped carbon sponges (NCS) through carbonization of metal-organic frameworks (MOFs) [92]. The unique pore structure trapped sulfur efficiently owing to hierarchically porous carbon materials derived from MOFs. Similarly, He et al. developed Co-doped with cobalt and nitrogen (C–Co–N) porous hosts for Li–Se batteries, which were also prepared with MOFs [93]. They substantiated that the well-performed cathodes with significantly decreased capacity decay can be result from the architecture and composition of C–Co–N skeleton to a great extent.

He's group further developed a porous Co–N–C scaffold derived from MOFs for the encapsulation of $SeS_2$ (Fig. 6(a)) [94]. The carbon host had adequate micropores and mesopores, which solved the problem of low areal loading for Li–$Se_xS_y$ batteries (66.5 wt% of $SeS_2$). Benefited from sufficient pore structures, the greatly conductive Co–N–C host acted as effective pathways for electron transportation and barriers to avoid the dissolution of intermediates into electrolyte. Besides, the homogenous location of Co and N nanoparticles fix the polysulfides and polyselenides because of strong chemical interactions. In Fig. 6(b), Co–N–C/$SeS_2$ delivered an initial specific capacity of 1153.5 mA h $g^{-1}$ at 0.2 C and stabilized in the following cycles. After 200 cycles, the capacity maintained 970.2 mA h $g^{-1}$, exhibiting a great capacity reservation of 84.1%. Electrochemical impedance spectroscopy (EIS) was employed and demonstrated that $R_{ct}$ of Co–N–C/$SeS_2$ was well below SP/$SeS_2$ and SP–Co/$SeS_2$, which further confirmed the synergistic catalytic effect of Co–N–C for redox reactions (Fig. 6(c)).

Guo et al. fabricated double-walled N-doped carbon@$NiCo_2S_4$ hollow capsules ($NiCo_2S_4$@NC) as host materials to confine $SeS_2$, thus achieved excellent performance of Li-$SeS_2$ battery as shown in Fig. 6(d) [95]. It has been studied that the high conductive hollow structure provided enough sites for nanoscale reactions and accommodated volume changes when cycling and the hollow capsules with $NiCo_2S_4$ lining and NC coating effectively constrain the shuttle effect by physical confinement and chemical absorption of polysulfides and polyselenides. Besides, $NiCo_2S_4$ with high polarity enhanced the (de)lithiation reaction kinetics. As can be seen from Fig. 6(e), the developed cathode demonstrated excellent rate performance (1205.1 mA h $g^{-1}$ at 0.1 C and 673.5 mA h $g^{-1}$ at 2.0 C) and long cycling life (800 cycles at 1.0 C).

For many reported Se-based electrodes, additional additives like conductive carbon and binders have been commonly added to enhance their electrochemical conductivity, however, they will decrease the mass percentage of active materials. Therefore, it is necessary and meaningful to develop flexible, free-standing and binder-free hosts [19,96]. Furthermore, the cell packing process can be greatly simplified by using such a configuration. Many freestanding electrodes have been constructed using nanofibers, nanotubes or nanobelts as scaffolds via a series of processes including electrospinning, templating, freeze-drying and vacuum filtration [97–101].

As shown in Fig. 6(f), Zhang and co-workers fabricated a binder-free lotus root-like carbon composite with $CoS_2$ decoration ($CoS_2$@LRC) [102]. Benefited from the interconnected multichannel carbon fibers, the cathode contained high proportion of $SeS_2$ (70 wt%) as no binder or other conductive additive was needed, as well as permit good electron transfer for a higher capacity utilization. In addition, the existence of $CoS_2$ nanoparticles all around the internal walls and external surfaces of LRC host provided enough areas for limiting the dissolution to restrain the shuttle phenomenon and maintain good cycling performance (over 400 cycles at 0.5 A $g^{-1}$).

It is also rational to take advantage of the formation and interaction of chemical bonds corresponding to additive transition metal element [103]. For instance, Lou's group fabricated a hollow mesoporous carbon@titanium nitride (HMC@TiN) host with 70 wt% load of active material as an electrode in the Fig. 6(g) [104]. HMC@TiN/$SeS_2$ demonstrated a high Coulombic efficiency (over 99%) since the second cycle, which revealed the dissolution of

Please cite this article in press as: H. Du, et al., J. Mater. Sci. Technol. (2020), https://doi.org/10.1016/j.jmst.2020.01.001

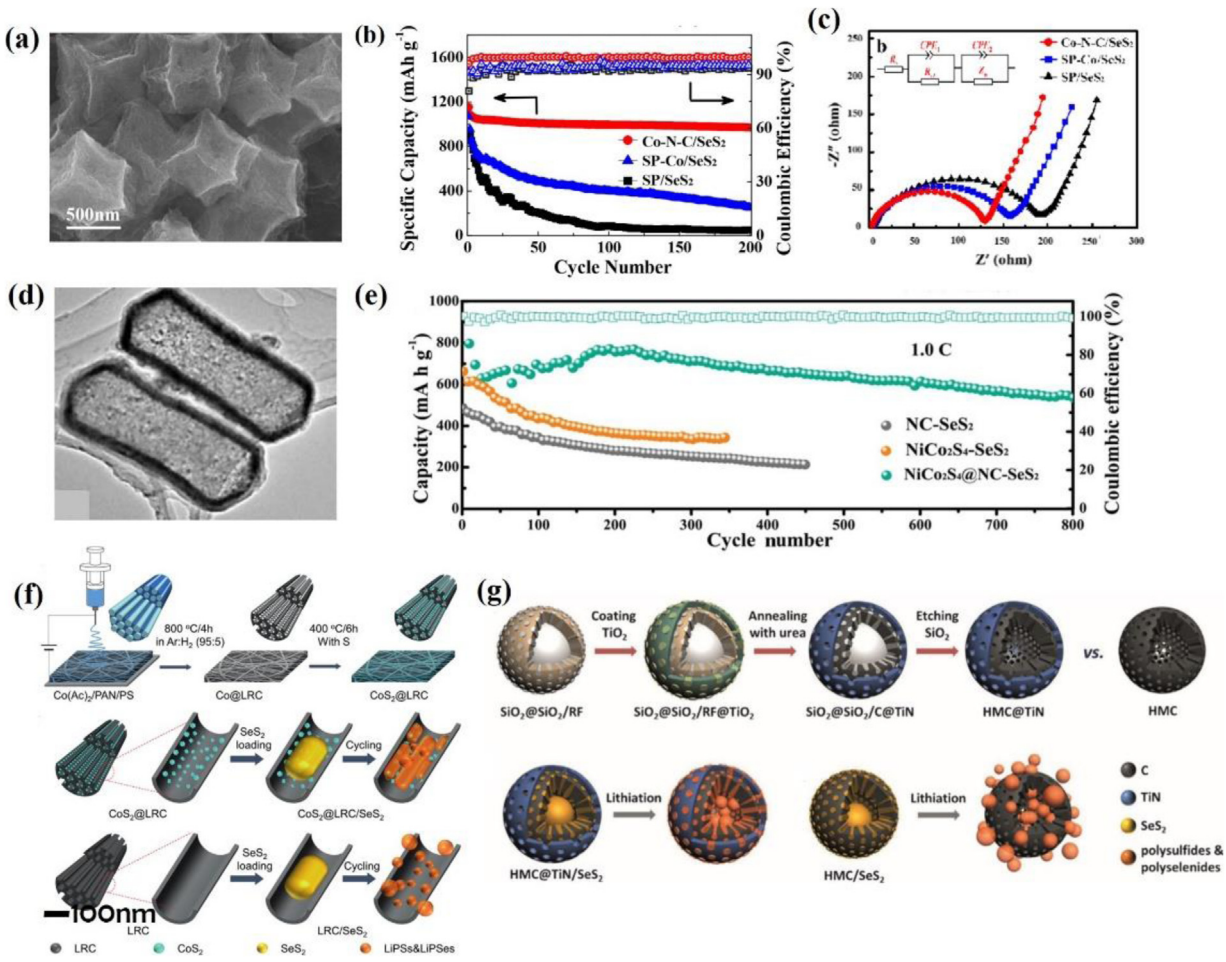


**Fig. 6.** (a) SEM image of Co-N-C/$SeS_2$, (b) cycling performance of SP/$SeS_2$, SP-Co/$SeS_2$ and Co-N-C/$SeS_2$ at 0.2 C and (c) EIS curves of the SP/$SeS_2$, SP-Co/$SeS_2$ and Co–N–C/$SeS_2$ after 200 cycles [94]. (d) TEM image of $NiCo_2S_4$@NC and (e) long-term cycling performances of $NiCo_2S_4$@NC–$SeS_2$, $NiCo_2S_4$–$SeS_2$ and NC–$SeS_2$ cathodes at 1.0C [95]. (f) Schematic synthesis model of $CoS_2$@LRC and advantages of $CoS_2$@LRC/$SeS_2$ over LRC/$SeS_2$ [102]. (LiPSs: lithium polysulfides, LiPSes: lithium polyselenides) (g) Schematic synthesis model of HMC@TiN [104].

polysulfides and polyselenides effectively controlled. On the contrary, HMC/$SeS_2$ cathode displayed not only faster capacity fading but also lower Coulombic efficiency in the same test conditions. The great contrast can be explained by the formation of Ti–S and N–S bonds, which guaranteed the effectively adsorption of polysulfides by the polar surface of TiN [105–107]. Moreover, the highly conductive TiN shell could efficiently limit the dissolution of polyselenides and polysulfides, as well as accelerate the transformation of long-chain polysulfides into short-chain polysulfides to improve the reaction kinetics of the HMC@TiN/$SeS_2$ electrode.

### 3.6. Optimization of Se/S ratio

Se and S are the same group elements in the periodic table and they are infinitely miscible. A large amount of $Se_xS_y$ solid solutions are available now, including $Se_5S$, $Se_5S_2$, $Se_5S_4$, SeS, $SeS_2$, $SeS_7$, and $SeS_{20}$, and thus they stand for a series of new-type cathode materials [20]. The more the introduction of S component, the higher capacity the cathode will get, in the meantime, the more the introduction of Se component, the more enhanced conductivity and reaction kinetics will be realized. In this regard, it is meaningful to find a rational molar ratio of S and Se to balance the capacity and conductivity and guarantee an optimal $Se_xS_y$ cathode material among all the possible $x/y$ values.

To investigate the best Se/S ratio for $Se_xS_y$ cathode, Wei et al. prepared a series of $Se_xS_y$/MCM composites, including $SeS_5$, $Se_2S_5$ and $Se_4S_5$ [22]. They conducted cycling and rate performance tests for the synthetic $Se_xS_y$/MCM composites in order to figure out the connection between different cathode compositions and their performance. As can be seen when cycling at 0.5 C in Fig. 7(a), the discharge capacity raised with the increasing S content for the first 20 cycles, due to the higher theoretical capacity of S than Se. In the following cycles, $Se_2S_5$/MCM and $Se_4S_5$/MCM cathode demonstrated a nearly 100% Coulombic efficiency and capacity retention of over 60%, however, $SeS_5$/MCM exhibited lower Coulombic efficiency and a faster capacity decay. As for rate capability (Fig. 7(b)), although $Se_2S_5$/MCM delivered similar capacities with $SeS_5$/MCM at medium current densities, it is clear that $Se_2S_5$/MCM exhibited better rate performance at higher current densities such as 2 C and 5 C and $Se_4S_5$/MCM performed the most unsatisfactory. Among the three $Se_xS_y$/MCM composites, $Se_2S_5$/MCM exhibited the most impressive result on capacity retention, Coulombic efficiency and rate performance.

Sun et al. also compared the cycle and rate performance between the $Se_nS_{8-n}$/ NMC ($n = 1 - 3$) and S/NMC composites [58]. As shown in Fig. 7(c), it was found the $Se_2S_6$/NMC sample showed the superior performance including the excellent discharge capacity (883 mA h $g^{-1}$) after 100 cycles. Besides, because of the difference of the theoretical capacity, an obvious decrease in the specific capacity was tested when changing $Se_2S_6$ to $Se_3S_5$. In Fig. 7(d), $Se_2S_6$/NMC also demonstrated better rate ability than the rest, showing a high rate capacity even at the maximum 5 A $g^{-1}$ (525 mA h $g^{-1}$). In

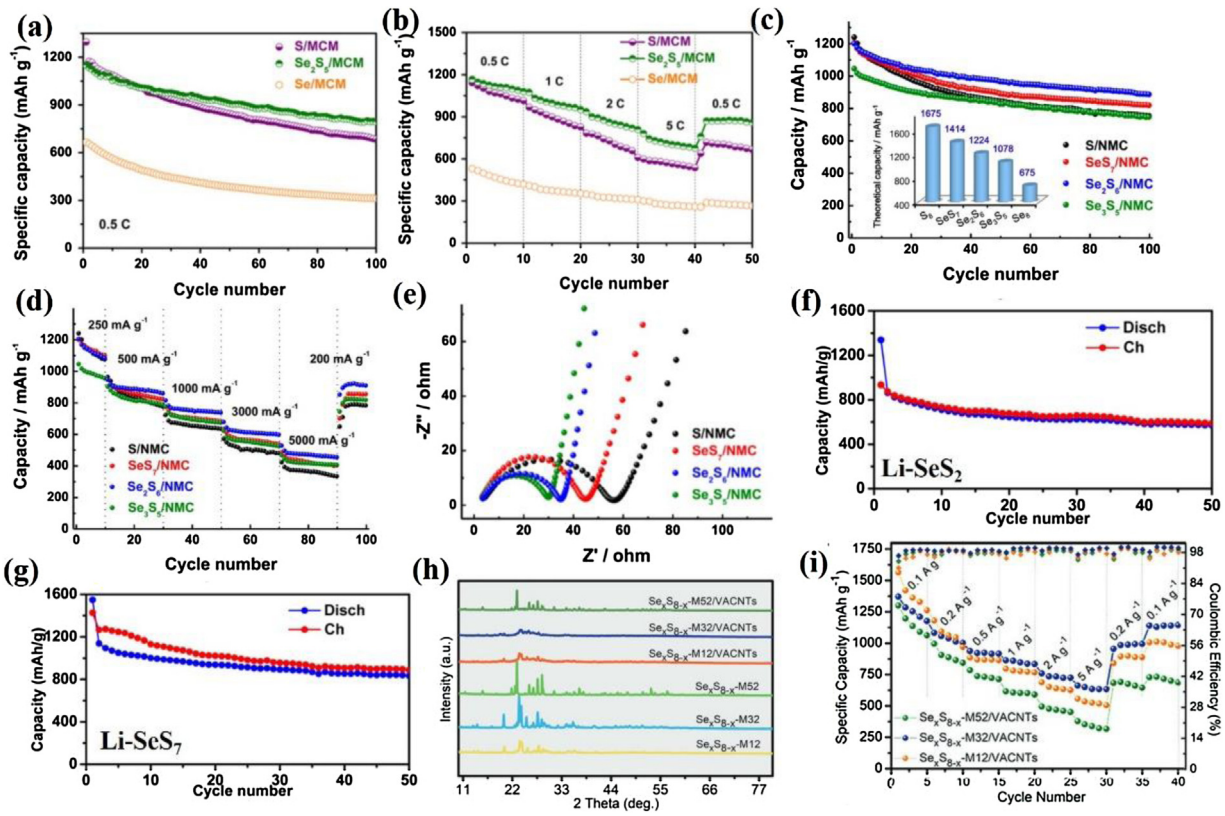


**Fig. 7.** (a) Cycling performance and (b) rate performance of $Se_4S_5$/MCM, $Se_2S_5$/MCM and $SeS_5$/MCM [22]. (c) Cycling performance, (d) rate performances and (e) EIS test of $Se_nS_{8-n}$/ NMC ($n = 1–3$) [58]. Cycling performance of (f) $SeS_2$/C and (g) $SeS_7$/C composite as cathodes [27]. (h) XRD patterns and (i) rate capability of the $Se_xS_{8-x}$/VACNTs cathodes [77].

addition, $Se_2S_6$/NMC showed a relatively lower charge transfer resistance in the EIS test, which further revealed good reaction kinetics owing to enhanced electronic transport properties of the $Se_2S_6$/NMC (Fig. 7(e)). Among the three $Se_xS_y$/NMC composites with different Se/S ratios, $Se_2S_6$/NMC demonstrated the optimal performance on discharge capacity, rate performance and kinetic behavior.

Cui and his co-workers have also tested the cycling performance of different kinds of cathodes including Se, $SeS_2$ and $SeS_7$ combined with CNTs as can be seen in Fig. 7(f) and (g) [27]. Benefited from the S component of high capacity, the first discharge capacity increased with increasing S content, which the Se, $SeS_2$ and $SeS_7$ cathodes delivered 350, 571 and 833 mA h $g^{-1}$, respectively. However, Li–$SeS_7$ battery exhibited a much lower Coulombic efficiency for the first 20 cycles than a nearly 100% Coulombic efficiency of the Li–$SeS_2$ batteries, which could be explained by overmuch S content in the $SeS_7$ cathode. Among three samples tested in this study, $SeS_2$ displayed the most balanced performance between discharge capacity and Coulombic efficiency

Fan et al. fabricated a series of $Se_xS_{8-x}$ cathodes with a set of Se/S ratios of 5/2, 3/2 and 1/2 (denoted as $Se_xS_{8-x}$-M52, $Se_xS_{8-x}$-M32, and $Se_xS_{8-x}$-M12, respectively) [77]. In the X-ray diffraction (XRD) test, a weak signal of $Se_xS_{8-x}$-M32 was shown in $Se_xS_{8-x}$-M32/VACNTs, which can be attributed to effective confinement of active materials in the inner space (Fig. 7(h)). However, active materials with Se/S ratios of 1/2 and 5/2 exhibited difficult perfusion into CNTs and they found them more likely to exist on the surfaces of the CNTs. The rate performance showed the consistent result with the XRD pattern, in which the $Se_xS_{8-x}$M32/VACNTs cathode demonstrated an obvious superior rate capability than the others (Fig. 7(i)). It delivered a high capacity (1404.5 mA h $g^{-1}$) at 0.1 A $g^{-1}$ with a high Coulombic efficiency (93%) and maintained 969 mA h $g^{-1}$ while returning to 0.1 A $g^{-1}$.

## 4. Electrolytes

Electrolyte plays a crucial role in the cathode interfacial electrochemistry of Li–$Se_xS_y$ battery systems and it has been proven that appropriate choice of electrolytes makes a difference on the electrochemical performance. There are two kinds of primary electrolytes applied in recent research for LIBs. Ether-based electrolytes are commonly investigated and used, which are Li salt dissolved in ether compounds. Unfortunately, polysulfides and polyselenides possess solubility in ether-based electrolytes and these electrolytes are not able to work well in some extreme conditions [108,109]. Carbonate-based electrolytes, the dominant alternative in lithium storage system, are absolutely another kind of candidates. However, they are chemically incompatible with the polysulfides [109–111]. In addition, there are other types of new-generation electrolytes including all-solid-state electrolytes [112–114] and solid/liquid hybrid electrolytes [115–117], which all have different impacts on the battery performance. Therefore, it is necessary to judge and compare the different electrolytes along with considering of the compatibility of specific electrode to specific electrolyte.

### 4.1. Carbonate-based electrolyte

In carbonate-based electrolytes, Se-based cathode can demonstrate superior electrochemical performance easily by confining Se in an appropriate conductive host, which can be explained by the effective limitation and stabilization of the production of intermediates to prevent the shuttle phenomenon. For instance, by using

mesoporous carbon material as cathode, Li – Se battery exhibited a stable reversible capacity (650 mA h $g^{-1}$), which is highly close to its theoretical value (675 mA h $g^{-1}$) [118].

Another noteworthy feature is the formation of SEI films in carbonate-based electrolytes, which is regarded as a critical factor to protect the cathode material and avoid the reaction between cathode materials and carbonyl groups [89,119]. Li et al. fabricated the Se/porous carbon nanospheres (PCN) composite and they found the immediate generation of SEI film containing F and O in the first charge process, as shown in the elemental mappings (Fig. 8(a), (b)) [53]. Due to the structure stability of carbon hosts, the formed SEI films were stable enough to relieve the volume changes of cathode during cycling. After stabilization, the SEI films played a huge role in preventing capacity loss. The porous structure and SEI films synergistically affected the material to preclude the polyselenides from dissolution into the electrolyte. Therefore, carbonate-based electrolytes could provide SEI films for better performance of Se-based batteries.

Nevertheless, not all SEI films can be beneficial to lithium batteries because of unstable SEI films and Li dendrite generated on the Li surface owing the inevitable reaction between Li and carbonate-based electrolyte, which greatly limit the cycling property [120]. Previous research reported that introducing proper additives can constrain the Li dendrite growth and immobilize the SEI films [121–123]. Guo's group introduced a controllable $AlCl_3$ to carbonate-based electrolyte [124]. The reaction between $AlCl_3$ and trace water in the carbonate-based electrolyte formed a stable $Al_2O_3$-rich SEI film on Li anode and Al-based positively charged colloidal particles (PCCPs). PCCPs could not only form electrostatic shield, but also induce the ensuing Li deposition to the adjacent Li protruded regions, which could form a uniform morphology without Li dendrite as shown in the schematic model of Fig. 8(c).

In addition, carbonate-based electrolytes exhibit some weakness in some other respects. It was found that a shift to a higher energy position of Se K-edge of $Se_2S_5$/MPC in situ measurement corresponding to $Li_2Se$ at the first discharge process in carbonate-based electrolyte (Fig. 8(d)). But the absorption intensity of Se could not be regained in the end, which indicates a great loss of irreversible capacity. This may be caused by the poor compatibility between polysulfides and carbonate-based electrolyte, which further declines the cycling reversibility of the cathode materials. Moreover, even well encapsulated of active material in the conductive matrix, most of the S-based cathodes cannot exhibit good performance in carbonate-based electrolyte due to the reaction between nucleophilic sulfide anions and the carbonate-based solvents [125].

It is also reported that a high polarization of the $Se_xS_y$-based batteries in the carbonate-based electrolyte causes lower Coulombic efficiency [126,127]. Meanwhile, EIS measurement was conducted to compare the stability between carbonate-based electrolyte and ether-based electrolyte [27]. As can be seen in Fig. 8(e), the resistances of $R_e$ and $R_{ct}$ of the Li–Se battery remained obviously unchanged after 5 cycles, while $R_e$ was significantly increased in carbonate-based electrolyte after 5 cycles. This reveals the carbonate-based electrolyte is unstable for Li–$Se_xS_y$ batteries to some extent due to significant growth of the cell impedance, which is quite similar with the Li–$O_2$ and Li–S storage systems [128–130].

### 4.2. Ether-based electrolyte

As for ether-based electrolytes, it has been reported that they could accelerate the redox reactions and provide higher reversible capacity under normal conditions owing to the Li salts [37,131]. Nevertheless, these electrolytes have their disadvantage in terms of the cycle stability of cathode materials. This can be explained by the easy dissolution of polysulfides, leading to other problems including severe capacity loss and shuttle effect [111]. Compared to carbonate-based electrolytes, there are fewer reports focusing on Li–Se and Li–$Se_xS_y$ storage system in ether-based electrolytes.

Cui et al. released a detailed report of Li–Se battery in ether-based electrolytes, which turned out that the electrochemistry was partly changed into multistep reaction by ether-based electrolytes (Fig. 2(a)) [27]. The situ XANES spectra witnessed a shift of Se K-edge absorption to a high energy in discharging process and back to low energy again in charging process, which indicated the formation of polyselenides as shown in Fig. 9(a). As previous study reported, the electrochemical properties of Se-based batteries in ether-based electrolytes is quite similar to that of the S-based systems [21]. Based on Li–S battery, a large number of carbon hosts with diff ;erent architectures have been synthesized for Se-based and $Se_xS_y$-based cathodes to preclude the formation of polyselenides and prevent shuttle eff ;ect. However, as mentioned above, most of the Se-based and $Se_xS_y$-based cathode materials still experience severe capacity fading and serious shuttle eff ;ect.

Babu and Ramesha developed a nitrogen doped carbon tubes (N-CT) for Se-based batteries in ether-based electrolyte through melt diffusion method [47]. The N-CT with a large amount of micropores and small mesopores exhibited well in trapping Se. It is worth noting that a reduction of intensity peak in the first and second cycles and a completely disappearance of peak after 15 cycles were discovered and the subsequent plots show only one peak at 1.75 V (Fig. 9(b)). This behavior can be attributed to the volume confinement effect, in which Se present in micropores cannot form higher order polyselenides [125]. Furthermore, this indicates the transfer of multistep reaction proposed by Cui et al. in ether-based electrolyte to a single direct step to form $Li_2Se$ [132,133]. At 0.2 C and 1 C after 100 continuous cycles, it could maintain 403 mA h $g^{-1}$ and 368 mA h $g^{-1}$, respectively.

Under some specific conditions, $Se_xS_y$-based cathodes can still demonstrate good performance in ether-based electrolytes. Han et al. applied the coated reduced graphene oxide (RGO) into Se/mesoporous carbon (MCN) cathode for higher capacity and improved cycle stability to address the rapid capacity decay of Se/MCN [31]. The cycle life was also extended by applying a graphene-coated separator, owing to the localization effect of the highly soluble intermediates in the separator and prevention of further reactions with Li anode [134]. Besides, superconcentrated electrolytes are also feasible for the use of ether-based electrolytes, which have regarded as a new-type effective liquid electrolyte since they have many advantages such as high reaction stability and speed, low volatility and polysulfide dissolution [135]. Lee et al. fabricated Se-infiltrated carbide-derived carbon (Se-CDC) and they reported that the higher Se utilization and cycle stability could be achieved when ether-based electrolyte accommodated higher concentration of Li salt [136]. After 25 cycles, discharge capacity increased with the increasing Li salt concentration, except excessive Li salt concentration.

### 4.3. All-solid-state electrolyte and solid/liquid hybrid electrolyte

In recent years, all-solid-state electrolytes have been brought into focus and exhibited unique performance as a substitute of flammable organic liquid electrolytes for safer inorganic solid electrolytes, which significantly simplifies the battery design and precludes short-circuits by blocking Li dendrites [137–139]. For instance, Li et al. used Se–$Li_3PS_4$–C composite as a cathode and Li–Sn composite as an anode to fabricated an advanced all-solid-state Li–Se cell [140]. In addition, all-solid-state batteries only need directly stacking and can achieve a higher operating voltage and fewer volume waste, which are beneficial to vehicle applications. A schematic model of a typical battery is shown in Fig. 9(c), which consists of three layers, including Li–In alloy as a counter electrode,

Please cite this article in press as: H. Du, et al., J. Mater. Sci. Technol. (2020), https://doi.org/10.1016/j.jmst.2020.01.001

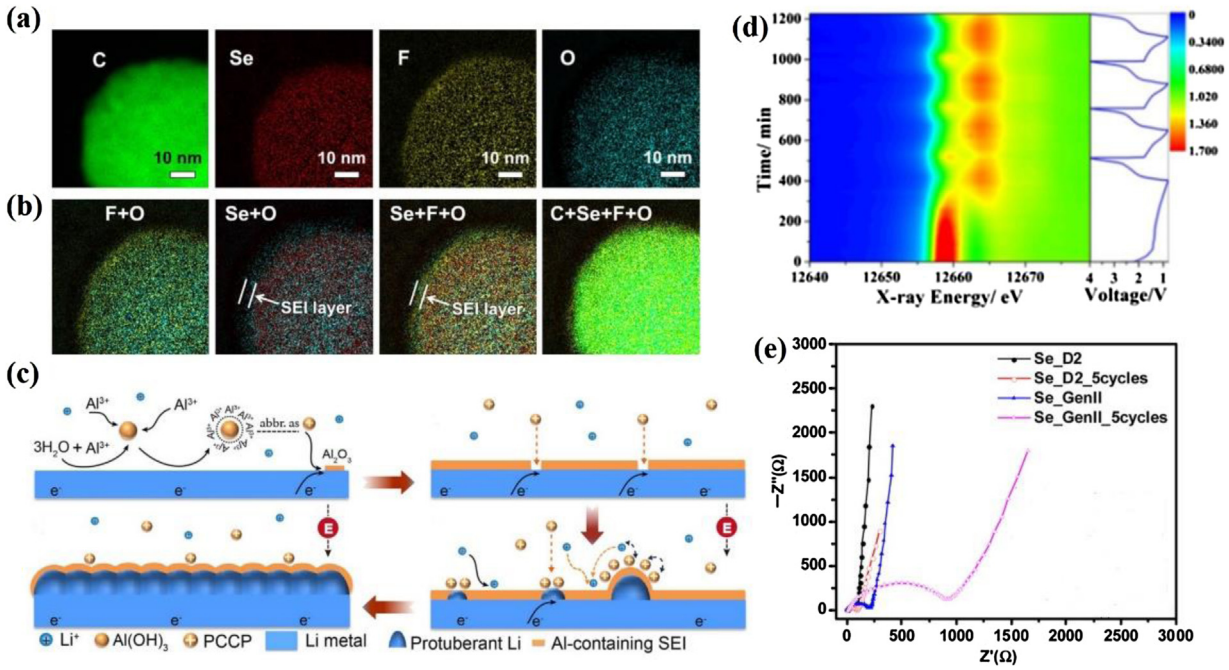


**Fig. 8.** (a) Elemental and (b) overlapped multi-elemental mappings after one cycle [53]. (c) Schematic model of $AlCl_3$ additive in the electrolyte [124]. (d) K-edge measurement of $Se_2S_5$/MPC in carbonate-based electrolyte [36]. (e) Nyquist plots of Li-Se battery with carbonate-based (GenII) and ether-based (D2) electrolytes after 5 cycles [27].

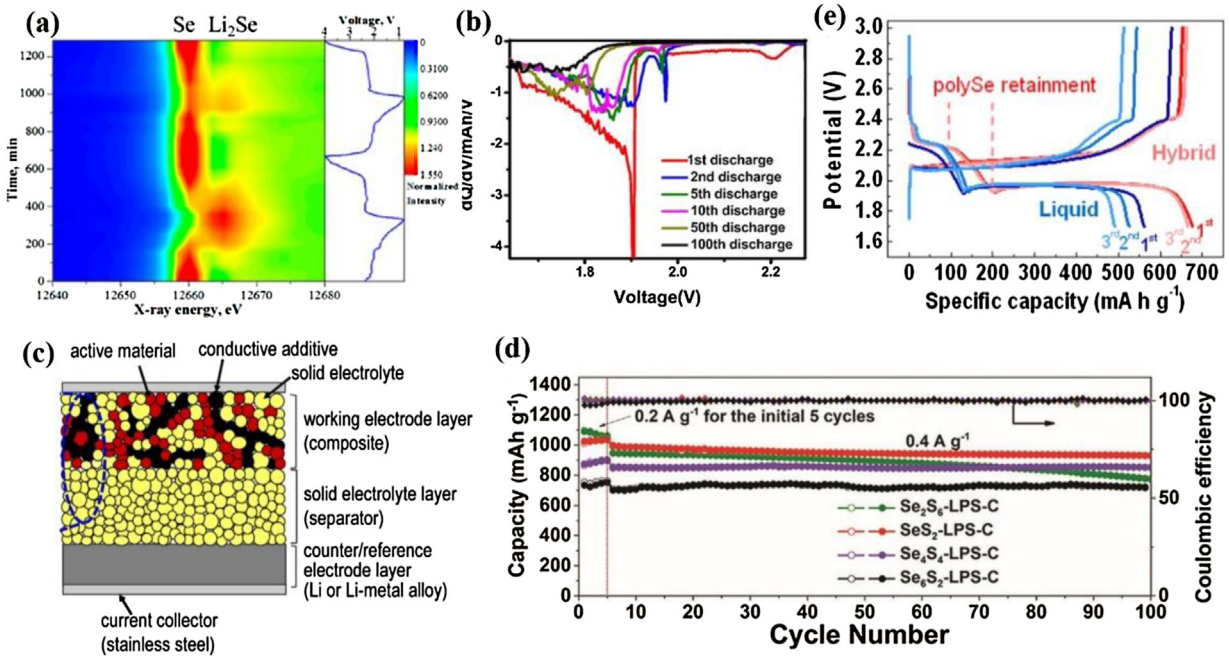


**Fig. 9.** (a) In situ XANES pattern of $Se_2S_5$/MPC at 0.2 C for the first and second cycle [36]. (b) dQ/dV differential curves of Se@N-CT-48 [47] (c) Schematic model of a typical all-solid-state electrochemical battery [141]. (d) Cycling performance of $SeS_x$–LPS–C at 0.4 A $g^{-1}$ [25]. (e) Voltage profiles of Li–Se batteries in hybrid electrolytes and liquid electrolyte at 0.1 C [25].

ceramic powder as a solid electrolyte and composite powder as a working electrode [141].

Sun et al. reported a feasible method to achieve high utilization of the stable cathode materials in all-solid-state lithium batteries (ASSLBs) to form $SeS_x$ solid solutions for the first time, which the interfacial ionic conductivity of prepared $SeS_x$–$Li_3PS_4$ composites was $10^{-6}$ S $cm^{-1}$ [25]. Among all prepared cathodes, the $SeS_2$/$Li_{10}GeP_2S_{12}$–$Li_3PS_4$/Li all-solid-state battery demonstrated outstanding performance of a high discharge capacity over 1100 mA h $g^{-1}$ at 50 mA $g^{-1}$ and a long cycling life for 100 cycles. In addition, the high $SeS_2$ loading battery delivered a reversible capacity of 12.6 mA h $cm^{-2}$, which reached the highest level of the advanced ASSLBs in this stage (Fig. 9(d)). All these findings extend the conventional knowledge on organic electrolytes to all-solid-state electrolytes for Li–$Se_xS_y$ batteries.

Because of the difficulty of forming efficient solid/solid interface and a high interfacial resistance of all-solid-state electrolytes and the inevitable shuttle effect of liquid-state electrolytes, the approach of combining the advantages of two kinds of electrolytes has attracted more attention [142–145]. Zhou et al.

reported an improved Li–Se battery assembled with hybrid electrolytes, which permitted quick liquid redox reactions and avoided shuttle effect [146]. The hybrid electrolyte was synthesized by $Li_{1.5}Al_{0.5}Ge_{1.5}(PO_4)_3$ (LAGP) ceramics surrounded by tetraethylene glycol dimethyl ether (TEGDME) electrolyte. Electrochemical test indicated that 677 mA h $g^{-1}$ could be reached at 0.1 C, demonstrating full utilization of Se cathode. In addition, the battery assembled with this electrolyte showed good cycling stability, which maintained 613 mA h $g^{-1}$ at 0.8 C over 500 cycles, corresponding to a capacity fading rate of 0.008 % per cycle (Fig. 9(e)).

### 4.4. Electrolyte additive and interlayer

Except that the inherent properties of the chosen electrolytes make a difference on the performance of Li–$Se_xS_y$ batteries, electrolyte additives also show great significance. $LiNO_3$ is the most applied electrolyte additive for conventional LIBs and also exhibits good performance in Li–$Se_xS_y$ system, which could limit the shuttle effect for an increased Coulombic efficiency, improved cycling stability and lower self-discharge rate [147,148]. By increasing Li salt concentration like adding $LiNO_3$, the anode stability can be improved and capacity decay can be effectively controlled. However, in Lou's research, when applying $LiNO_3$ on Li–$SeS_2$ battery, a passivation film was formed on the anode and an irreversible reduction was shown on the cathode [52]. This phenomenon decreased the cycling stability and increased the impedance of interfaces of the Li–$SeS_2$ batteries, which is also shown in previous reported Li–S batteries [149–151]. In this regard, the direction of future work should focus on balancing the capacity requirement and the side effects resulted from the introduction of $LiNO_3$.

In $Se_xS_y$-based storage system, the common shuttle effect leads to severe capacity decay and the migration of intermediates to the surface of Li anode, which would corrode the Li anode and form a passivation film. Some researchers developed protective interlayer, which remains permeable to $Li^+$ transfer but prevents the transportation of intermediates to improve cycle stability [152–156]. In addition, it is efficient to promote the polysulfides to form poorly soluble $Li_2S$ by introducing interlayer, thus further enhancing the electrochemical performance. Gu et al. fabricated a N-doped loofah sponge carbon (N-LSC) to be a multifunctional interlayer for Li–S and Li–Se batteries [157]. Benefited from high specific areas (2551.06 $m^2$ $g^{-1}$), superior conductivity (1170 S $m^{-1}$) and porous structure (1.75 $cm^3$ $g^{-1}$), Li–Se batteries assembled with N-LSC interlayer demonstrated outstanding electrochemical performance stability (350 mA h $g^{-1}$ after 1000 cycles). The well-performed N-LSC interlayer on Li–Se batteries also provides a solution on the future development of interlayer in $Se_xS_y$-based storage system.

## 5. Conclusion and perspective

Li–$Se_xS_y$ batteries have gained considerable attention in recent years since their first proposal in 2012. Understanding the reaction mechanism is necessary for the rational development and further study of high-performance Li–$Se_xS_y$ batteries. In ether-based electrolytes, two processes are discovered while discharging, corresponding to Se to $Li_2Se_n$ and $Li_2Se$ to $Li_2Se_n$. When it comes to carbonate-based electrolytes during discharging, only one process is discovered corresponding to Se to $Li_2Se$ without intermediate phases. Especially, most of the cathodes exhibit an obvious capacity decay in ether-based electrolyte even well confined in carbon host.

The architectural characteristics of carbon hosts have a pivotal effect on the electrochemical performance. According to the most successful cathodes reported to date, an ideal carbon matrix for $Se_xS_y$ hosting should have the following properties:

(1) Small pore size (micropores or small mesopores) for $Se_n^{2-}$/$S_n^{2-}$ trapping;

(2) The porosity structure being composed of uniform mesopores. Hollow structures are particularly attractive as an internal sulfur reservoir for more active material loading is better than spreading active materials throughout the cathode;

(3) High electrical conductivity and intimate contact with $Se_xS_y$;

(4) Chemical irregular carbon structure developed by doping or defect, which is better than an ideal graphitic $sp^2$ structure;

(5) A protect layer on top of the cathode that is a necessary factor, in which conductive polymers exhibit well in this regard;

(6) Robust or flexible skeleton to effectively bear the strain generated by volume expansion of $Se_xS_y$ during lithiation;

(7) low cost and easy for scale up.

As the ratio between Se and S is varied in $Se_xS_y$ solid solutions, the optimal $Se_xS_y$ materials with the specific Se/S ratio have a broad research prospect. The most suitable Se/S ratio can take advantages of both the cheap price, high capacity of S and high electrochemical activity, cycle stability of Se.

High sensitivity of the Li–$Se_xS_y$ batteries to the electrolytes has raised considerable researches of discovering the most suitable electrolyte. Se-based cathode in carbonate-based electrolyte exhibits lower shuttle phenomena and has a higher tendency to generate SEI films, while it is not very stable for Li–$Se_xS_y$ battery systems and the well-known poor compatibility between polysulfides and carbonate-based electrolytes decreases the reaction reversibility. High capacity fading is discovered in ether-based electrolytes even when $Se_xS_y$ is well encapsulated in a great amount of carbon hosts, which can be also solved by introducing other additives like reduced graphene oxide or adapting superconcentrated electrolytes. Li–$Se_xS_y$ batteries can work feasibly in both carbonate-based and ether-based electrolytes, although both of them have their own advantages and disadvantages. All-solid-state electrolytes have gained much more attention owing to the more simplified and safer structure, which also enable a higher operating voltage and cause fewer volume waste. Li–$Se_xS_y$ batteries assembled with all-solid-state electrolyte show excellent performance. New solid/liquid hybrid electrolytes have come into sight and showed their superiority than conventional electrolytes.

Recently, based on the Se–S chemistry, Te and S are also found to be miscible, representing a broad class of new-type electrode materials [158]. $Te_xS_y$-based cathodes are newly developed, which may become higher energy density batteries for transportation vehicles and grid applications. Compared to these different kind of cathode materials, anode materials are very single. Sodium, magnesium and potassium have not been deeply investigated for $Se_xS_y$ cathode materials.

This work reviews the research status of Li–$Se_xS_y$ batteries and mainly focuses on the design and synthesis of micro/nanostructured electrodes. Aimed at the key problems of Li–$Se_xS_y$ batteries, these researches put forward lots of solutions and optimum proposals. Although there remains many difficulties and challenges, with the deepening of our understanding of Li–$Se_xS_y$ batteries, and with the help of advanced characterization methods and research methods, we can design and develop newly high-performance $Se_xS_y$ material. Instead, significance of further research should be attached on maximizing the advantages of Li–$Se_xS_y$ batteries and minimizing the cost of $Se_xS_y$-based storage system.

The Li–$Se_xS_y$ system is a new battery system holding great promise, which may assist in developing advanced rechargeable batteries with enhanced energy density and safety, and stepping toward to the application of advanced batteries in electric vehicles and stationary energy storage. It is expected that this review can enhance and deepen our fundamental understanding

Please cite this article in press as: H. Du, et al., J. Mater. Sci. Technol. (2020), https://doi.org/10.1016/j.jmst.2020.01.001

of structure-electrochemical performance correlation, and advance our knowledge in nanotechnology and material science.

## Acknowledgments

This work was financially supported by the National Natural Science Foundation of China (Nos. 51832004 and 51904216), the National Natural Science Fund for Distinguished Young Scholars (No. 51425204), the National Students Innovation and Entrepreneurship Training Program (WUT: 20191049721017), the National Key R&D Program of China (No. 2016YFA0202603), the Programme of Introducing Talents of Discipline to Universities (No. B17034), the Yellow Crane Talent (Science & Technology) Program of Wuhan City and the Fundamental Research Funds for the Central Universities (WUT: 193114007).

## References

[1] J. Meng, H. Guo, C. Niu, Y. Zhao, L. Xu, Q. Li, L. Mai, Joule 1 (2017) 522–547.
[2] L. Zhou, K. Zhang, Z. Hu, Z. Tao, L. Mai, Y.M. Kang, S.L. Chou, J. Chen,Adv. Energy Mater. 8 (2018), 1701415.
[3] A.W. Anwar, A. Majeed, N. Iqbal, W. Ullah, A. Shuaib, U. Ilyas, F. Bibi, H.M. Rafique, J. Mater. Sci. Technol. 31 (2015) 699–707.
[4] P.K. Choubey, K.S. Chung, M.S. Kim, J.C. Lee, R.R. Srivastava, Miner. Eng. 110 (2017) 104–121.
[5] J. El Haddad, L. Canioni, B. Bousquet, Spectrochim. Acta B 101 (2014) 171–182.
[6] T.C. Nirmale, B.B. Kale, A.J. Varma, Int. J. Biol. Marcomol. 103 (2017) 1032–1043.
[7] X. Zeng, J. Li, L. Liu, Renew Sust. Energ. Rev. 52 (2015) 1759–1767.
[8] W. Luo, J.J. Gaumet, L. Mai, Rare Met. 36 (2017) 321–338.
[9] B.D. McCloskey, A. Speidel, R. Scheffler, D.C. Miller, V. Viswanathan, J.S. Hummelshoj, J.K. Norskov, A.C. Luntz, J. Phys. Chem. Lett. 3 (2012) 997–1001.
[10] Y. Zhao, L. Xu, L. Mai, C. Han, Q. An, X. Xu, X. Liu, Q. Zhang, P. Natl. Acad. Sci. USA 109 (2012) 19569–19574.
[11] J. Chen, R. Yuan, J. Feng, Q. Zhang, J. Huang, G. Fu, M. Zheng, B. Ren, Q. Dong, Chem. Mater. 27 (2015) 2048–2055.
[12] A. Eftekhari, D.W. Kim, J. Mater. Chem. A 5 (2017) 17734–17776.
[13] X. Liu, J. Huang, Q. Zhang, L. Mai,Adv. Mater. 29 (2017), 1601759.
[14] M.M. Thackeray, C. Wolverton, E.D. Isaacs, Energy Environ. Sci. 5 (2012) 7854.
[15] V.S. Saji, C.W. Lee, RSC Adv. 3 (2013) 10058.
[16] A. Eftekhari, Sustain. Energy Fuels 1 (2017) 14–29.
[17] J. Jin, X. Tian, N. Srikanth, L.B. Kong, K. Zhou, J. Mater. Chem. A 5 (2017) 10110–10126.
[18] C. Yang, Y. Yin, Y. Guo, J. Phys. Chem. Lett. 6 (2015) 256–266.
[19] Z. Zhang, Z. Zhang, K. Zhang, X. Yang, Q. Li, RSC Adv. 4 (2014) 15489–15492.
[20] A. Abouimrane, D. Dambournet, K.W. Chapman, P.J. Chupas, W. Weng, K. Amine, J. Am. Chem. Soc. 134 (2012) 4505–4508.
[21] G.L. Xu, J. Liu, R. Amine, Z. Chen, K. Amine, ACS Energy Lett. 2 (2017) 605–614.
[22] Y. Wei, Y. Tao, Z. Kong, L. Liu, J. Wang, W. Qiao, L. Ling, D. Long, Energy Storage Mater. 5 (2016) 171–179.
[23] H. Liu, H. Yu, J. Mater. Sci. Technol. 35 (2019) 674–686.
[24] C. Barchasz, J.C. Leprêtre, S. Patoux, F. Alloin, Electrochim. Acta 89 (2013) 737–743.
[25] X. Li, J. Liang, J. Luo, C. Wang, X. Li, Q. Sun, R. Li, L. Zhang, R. Yang, S. Lu, H. Huang, X. Sun,Adv. Mater. 31 (2019), 1808100.
[26] Y. Cui, A. Abouimrane, C.J. Sun, Y. Ren, K. Amine, Chem. Commun. 50 (2014) 5576–5579.
[27] Y. Cui, A. Abouimrane, J. Lu, T. Bolin, Y. Ren, W. Weng, C. Sun, V.A. Maroni, S.M. Heald, K. Amine, J. Am. Chem. Soc. 135 (2013) 8047–8056.
[28] B. Scrosati, J. Hassoun, Y.K. Sun, Energy Environ. Sci. 4 (2011) 3287–3295.
[29] Z. Zhang, S. Jiang, Y. Lai, J. Li, J. Song, J. Li, J. Power Sources 284 (2015) 95–102.
[30] J. Guo, Z. Wen, G. Ma, J. Jin, W. Wang, Y. Liu, RSC Adv. 5 (2015) 20346–20350.
[31] K. Han, Z. Liu, J. Shen, Y. Lin, F. Dai, H. Ye, Adv. Funct. Mater. 25 (2015) 455–463.
[32] S. Jiang, Z. Zhang, Y. Lai, Y. Qu, X. Wang, J. Li, J. Power Sources 267 (2014) 394–404.
[33] Y. Qu, Z. Zhang, Y. Lai, Y. Liu, J. Li, Solid State Ionics 274 (2015) 71–76.
[34] X. Wang, Z. Zhang, X. Yan, Y. Qu, Y. Lai, J. Li, Electrochim. Acta 155 (2015) 54–60.
[35] Z. Zhang, X. Yang, X. Wang, Q. Li, Z. Zhang, Solid State Ionics 260 (2014) 101–106.
[36] G. Xu, T. Ma, C. Sun, C. Luo, L. Cheng, Y. Ren, S.M. Heald, C. Wang, L. Curtiss, J. Wen, D.J. Miller, T. Li, X. Zuo, V. Petkov, Z. Chen, K. Amine, Nano Lett. 16 (2016) 2663–2673.
[37] S. Chen, Y. Zhai, G. Xu, Y. Jiang, D. Zhao, J. Li, L. Huang, S. Sun, Electrochim. Acta 56 (2011) 9549–9555.
[38] Q. Zhang, Y. Wang, Z.W. Seh, Z. Fu, R. Zhang, Y. Cui, Nano Lett. 15 (2015) 3780–3786.
[39] H. Chen, C. Wang, W. Dong, W. Lu, Z. Du, L. Chen, Nano Lett. 15 (2015) 798–802.
[40] L. Fei, X. Li, W. Bi, Z. Zhuo, W. Wei, L. Sun, W. Lu, X. Wu, K. Xie, C. Wu, H.L. Chan, Y. Wang, Adv. Mater. 27 (2015) 5936–5942.
[41] M. Ge, J. Rong, X. Fang, C. Zhou, Nano Lett. 12 (2012) 2318–2323.
[42] W. Li, F. Wang, S. Feng, J. Wang, Z. Sun, B. Li, Y. Li, J. Yang, A.A. Elzatahry, Y. Xia, D. Zhao, J. Am. Chem. Soc. 135 (2013) 18300–18303.
[43] J. Liu, K. Song, P.A. van Aken, J. Maier, Y. Yu, Nano Lett. 14 (2014) 2597–2603.
[44] M. Jia, Y. Niu, C. Mao, S. Liu, Y. Zhang, S.J. Bao, M. Xu, J. Colloid. Interf. Sci. 490 (2017) 747–753.
[45] C. Zhao, S. Fang, Z. Hu, S. Qiu, K. Liu, J. Nanopart. Res. 18 (2016) 201.
[46] B. Zhang, X. Qin, G.R. Li, X. Gao, Energy Environ. Sci. 3 (2010) 1531.
[47] D.B. Babu, K. Ramesha, Electrochim. Acta 219 (2016) 295–304.
[48] S. Xin, L. Gu, N.H. Zhao, Y.X. Yin, L.J. Zhou, Y.G. Guo, L.J. Wan, J. Am. Chem. Soc. 134 (2012) 18510–18513.
[49] Y. Liu, L. Si, X. Zhou, X. Liu, Y. Xu, J. Bao, Z. Dai, J. Mater. Chem. A 2 (2014) 17735–17739.
[50] Y. Liu, X. Zhao, G.S. Chauhan, J.H. Ahn, Appl. Surf. Sci. 380 (2016) 151–158.
[51] X. Li, Y. Cao, W. Qi, L.V. Saraf, J. Xiao, Z. Nie, J. Mietek, J. Zhang, B. Schwenzer, J. Liu, J. Mater. Chem. 21 (2011) 16603.
[52] Z. Li, J. Zhang, H. Wu, X. Lou,Adv. Energy Mater. 7 (2017), 1700281.
[53] Z. Li, L. Yuan, Z. Yi, Y. Liu, Y. Huang, Nano. Energy 9 (2014) 229–236.
[54] X. Li, J. Liang, K. Zhang, Z. Hou, W. Zhang, Y. Zhu, Y. Qian, Energy Environ. Sci. 8 (2015) 3181–3186.
[55] N. Liu, J. Shen, D. Liu, Electrochim. Acta 97 (2013) 271–277.
[56] J. Wang, S. Kaskel, J. Mater. Chem. 22 (2012) 23710.
[57] Z. Zhang, Z. Li, F. Hao, X. Wang, Q. Li, Y. Qi, R. Fan, L. Yin, Adv. Funct. Mater. 24 (2014) 2500–2509.
[58] F. Sun, H. Cheng, J. Chen, N. Zheng, Y. Li, J. Shi, ACS Nano 10 (2016) 8289–8298.
[59] G. Zheng, Y. Yang, J.J. Cha, S.S. Hong, Y. Cui, Nano Lett. 11 (2011) 4462–4467.
[60] S. Chen, X. Huang, B. Sun, J. Zhang, H. Liu, G. Wang, J. Mater. Chem. A 2 (2014) 16199–16207.
[61] N. Jayaprakash, J. Shen, S.S. Moganty, A. Corona, L.A. Archer, Angew. Chem. Int. Edit. 50 (2011) 5904–5908.
[62] C. Zhang, C. Yuan, Z. Guo, X. Lou, Angew. Chem. Int. Edit. 51 (2012) 9592–9595.
[63] G. He, X. Liang, M. Cuisinier, A. Garsuch, L.F. Nazar, ACS Nano 7 (2013) 10920–10930.
[64] W. Luo, D. Guan, R. He, F. Li, L. Mai, Acta. Phys.-Chim. Sin. 32 (2016) 1999–2006.
[65] H. Zhang, L. Zhou, X. Huang, H. Song, C. Yu, Nano Res. 9 (2016) 3725–3734.
[66] K. Balakumar, N. Kalaiselvi, Carbon 112 (2017) 79–90.
[67] X. Wang, Z. Zhang, Y. Qu, G. Wang, Y. Lai, J. Li, J. Power Sources 287 (2015) 247–252.
[68] L. Zeng, W. Li, Y. Jiang, Y. Yu, Rare Met. 36 (2017) 339–364.
[69] Y. Yao, L. Zeng, S. Hu, Y. Jiang, B. Yuan, Y. Yu,Small 13 (2017), 1603513.
[70] C. Liang, N.J. Dudney, J.Y. Howe, Chem. Mater. 21 (2009) 4724–4730.
[71] T.H. Hwang, D.S. Jung, J.S. Kim, B.G. Kim, J.W. Choi, Nano Lett. 13 (2013) 4532–4538.
[72] G.P. Pandey, K. Jones, L. Meda, MRS Adv. 4 (2019) 821–828.
[73] J. Meng, C. Niu, L. Xu, J. Li, X. Liu, X. Wang, Y. Wu, X. Xu, W. Chen, Q. Li, Z. Zhu, D. Zhao, L. Mai, J. Am. Chem. Soc. 139 (2017) 8212–8221.
[74] J.A. Syed, J. Ma, B. Zhu, S. Tang, X. Meng,Adv. Energy Mater. 7 (2017), 1701228.
[75] G. Tan, F. Wu, Y. Yuan, R. Chen, T. Zhao, Y. Yao, J. Qian, J. Liu, Y. Ye, R. Shahbazian-Yassar, J. Lu, K. Amine, Nat. Commun. 7 (2016) 11774.
[76] C. Tang, Q. Zhang, M. Zhao, J. Huang, X. Cheng, G. Tian, H. Peng, F. Wei, Adv. Mater. 26 (2014) 6100–6105.
[77] H. Fan, S. Chen, X. Chen, Q. Tang, A. Hu, W. Luo, H. Liu, S. Dou,Adv. Funct. Mater. 28 (2018), 1805018.
[78] D. Kundu, F. Krumeich, R. Nesper, J. Power Sources 236 (2013) 112–117.
[79] J. Zhang, Y. Xu, L. Fan, Y. Zhu, J. Liang, Y. Qian, Nano Energy 13 (2015) 592–600.
[80] J. Wang, Y. He, J. Yang, Adv. Mater. 27 (2015) 569–575.
[81] L. Wang, X. He, J. Li, J. Gao, J. Guo, C. Jiang, C. Wan, J. Mater. Chem. 22 (2012) 22077.
[82] J. Fanous, M. Wegner, J. Grimminger, Ä. Andresen, M.R. Buchmeiser, Chem. Mater. 23 (2011) 5024–5028.
[83] S.S. Zhang, Front. Energy Res. 1 (2013) 1–9.
[84] Z. Li, Y. Lu, X. Lou, Sci. Adv. 4 (2018), eaat1687.
[85] J. Fanous, J. Grimminger, M. Rolff, M.B.M. Spera, M. Tenzerb, M.R. Buchmeiser, J. Mater. Chem. 22 (2012) 23240.
[86] J. Wang, C. Wan, K. Du, J. Xie, N. Xu, Adv. Funct. Mater. 13 (2003) 487–492.
[87] L. Yin, J. Wang, F. Lin, J. Yang, Y. Nuli, Energ. Environ. Sci. 5 (2012) 6966.
[88] J. Guo, Z. Yang, Y. Yu, H.D. Abruna, L.A. Archer, J. Am. Chem. Soc. 135 (2013) 763–767.
[89] C. Luo, Y. Wen, J. Wang, C. Wang, Adv. Funct. Mater. 24 (2014) 4082–4089.
[90] L. Liu, Y. Wei, C. Zhang, C. Zhang, X. Li, J. Wang, L. Ling, W. Qiao, D. Long, Electrochim. Acta 153 (2015) 140–148.
[91] Z. Yi, L. Yuan, D. Sun, Z. Li, C. Wu, W. Yang, Y. Wen, B. Shan, Y. Huang, J. Mater. Chem. A 3 (2015) 3059–3065.
[92] Z. Li, L. Yin, Nanoscale 7 (2015) 9597–9606.

[93] J. He, W. Lv, Y. Chen, J. Xiong, K. Wen, C. Xu, W. Zhang, Y. Li, W. Qin, W. He, J. Power Sources 363 (2017) 103–109.
[94] J. He, Y. Chen, J. Xiong, K. Wen, C. Xu, W. Zhang, Y. Li, W. Qin, W. He, J. Mater. Chem. A 6 (2018) 10466–10473.
[95] B. Guo, T. Yang, W. Du, Q. Ma, L. Zhang, S. Bao, X. Li, Y. Chen, M. Xu, J. Mater. Chem. A 7 (2019) 12276–12282.
[96] D. Huang, S. Li, Y. Luo, X. Xiao, L. Gao, M. Wang, Y. Shen, Electrochim. Acta 190 (2016) 258–263.
[97] Q. Cai, Y. Li, L. wang, Q. Li, J. Xu, B. Gao, X. Zhang, K. Huo, P.K. Chu, Nano Energy 32 (2017) 1–9.
[98] K. Han, Z. Liu, H. Ye, F. Dai, J. Power Sources 263 (2014) 85–89.
[99] J. He, Y. Chen, W. Lv, K. Wen, P. Li, Z. Wang, W. Zhang, W. Qin, W. He, ACS Energy Lett. 1 (2016) 16–20.
[100] L. Zeng, X. Wei, J. Wang, Y. Jiang, W. Li, Y. Yu, J. Power Sources 281 (2015) 461–469.
[101] L. Xu, Z. Jiang, L. Mai, Q. Qing, Nano Lett. 14 (2014) 3602–3607.
[102] J. Zhang, Z. Li, X. Lou, Angew. Chem. Int. Edit. 56 (2017) 14107–14112.
[103] Z. Li, Q. He, X. Xu, Y. Zhao, X. Liu, C. Zhou, D. Ai, L. Xia, L. Mai,Adv. Mater. 30 (2018), 1804089.
[104] Z. Li, J. Zhang, B. Guan, X. Lou, Angew. Chem. Int. Edit. 56 (2017) 16003–16007.
[105] Z. Cui, C. Zu, W. Zhou, A. Manthiram, J.B. Goodenough, Adv. Mater. 28 (2016) 6926–6931.
[106] Z. Hao, L. Yuan, C. Chen, J. Xiang, Y. Li, Z. Huang, P. Hu, Y. Huang, J. Mater. Chem. A 4 (2016) 17711–17717.
[107] T.G. Jeong, D.S. Choi, H. Song, J. Choi, S.A. Park, S.H. Oh, H. Kim, Y. Jung, Y.T. Kim, ACS Energy Lett. 2 (2017) 327–333.
[108] D. Aurbach, E. Pollak, R. Elazari, G. Salitra, C.S. Kelley, J. Affinito, J. Electrochem. Soc. 156 (2009) A694–A702.
[109] X. Li, A. Lushington, Q. Sun, W. Xiao, J. Liu, B. Wang, Y. Ye, K. Nie, Y. Hu, Q. Xiao, R. Li, J. Guo, T.K. Sham, X. Sun, Nano Lett. 16 (2016) 3545–3549.
[110] J. Gao, M.A. Lowe, Y. Kiya, H.D. Abruña, J. Phys. Chem. C 115 (2011) 25132–25137.
[111] T. Yim, M.S. Park, J.S. Yu, K.J. Kim, K.Y. Im, J.H. Kim, G. Jeong, Y.N. Jo, S.G. Woo, K.S. Kang, I. Lee, Y.J. Kim, Electrochim. Acta 107 (2013) 454–460.
[112] C.K. Chan, R. Ruffo, S.S. Hong, Y. Cui, J. Power Sources 189 (2009) 1132–1140.
[113] E. Quartarone, P. Mustarelli, Chem. Soc. Rev. 40 (2011) 2525.
[114] C. Sun, J. Liu, Y. Gong, D.P. Wilkinson, J. Zhang, Nano Energy 33 (2017) 363–386.
[115] Y. Lu, S.K. Das, S.S. Moganty, L.A. Archer, Adv. Mater. 24 (2012) 4430–4435.
[116] Y. Lu, K. Korf, Y. Kambe, Z. Tu, L.A. Archer, Angew. Chem. Int. Edit. 53 (2014) 488–492.
[117] Y. Wang, P. He, H. Zhou, Energ. Environ. Sci. 4 (2011) 4994.
[118] C. Yang, Y. Yin, H. Ye, J. Zhang, Y. Guo, Angew. Chem. Int. Edit. 52 (2013) 8263–8367.
[119] H. Ye, Y. Yin, S. Zhang, Y. Guo, J. Mater. Chem. A 2 (2014) 13293.
[120] D. Aurbach, J. Power Sources 89 (2000) 206–218.
[121] J. Qian, W. Xu, P. Bhattacharya, M. Engelhard, W.A. Henderson, Y. Zhang, J. Zhang, Nano Energy 15 (2015) 135–144.
[122] X. Zhang, X. Cheng, X. Chen, C. Yan, Q. Zhang,Adv. Funct. Mater. 27 (2017), 1605989.
[123] X. Yang, X. Li, K. Adair, H. Zhang, X. Sun, Electro. Chem. Energ. Rev. 1 (2018) 239–293.
[124] H. Ye, Y. Yin, S. Zhang, Y. Shi, L. Liu, X. Zeng, R. Wen, Y. Guo, L. Wan, Nano Energy 36 (2017) 411–417.
[125] Z. Li, L. Yuan, Z. Yi, Y. Sun, Y. Liu, Y. Jiang, Y. Shen, Y. Xin, Z. Zhang, Y. Huang,Adv. Energy Mater. 4 (2014), 1301473.
[126] P.W. Ruch, D. Cericola, A. Foelske, R. Kötz, A. Wokaun, Electrochim. Acta 55 (2010) 2352–2357.
[127] Y. Tominaga, K. Yamazaki, Chem. Commun. 50 (2014) 4448–4450.
[128] S. Das, J. Højberg, K.B. Knudsen, R. Younesi, P. Johansson, P. Norby, T. Vegge, J. Phys. Chem. C 119 (2015) 18084–18090.
[129] K. Kim, I. Park, S.Y. Ha, Y. Kim, M.H. Woo, M.H. Jeong, W.C. Shin, M. Ue, S.Y. Hong, N.S. Choi, Electrochim. Acta 225 (2017) 358–368.
[130] B. Li, M. Xu, T. Li, W. Li, S. Hu, Electrochem. Commun. 17 (2012) 92–95.
[131] L. Ma, H. Zhuang, Y. Lu, S.S. Moganty, R.G. Hennig, L.A. Archer,Adv. Energy Mater. 4 (2014), 1400390.
[132] Y. Liu, L. Si, Y. Du, X. Zhou, Z. Dai, J. Bao, J. Phys. Chem. C 119 (2015) 27316–27321.
[133] Y. Liu, L. Si, X. Zhou, X. Liu, Y. Xu, J. Bao, Z. Dai, J. Mater. Chem. A 2 (2014) 17735–17739.
[134] R. Fang, G. Zhou, S. Pei, F. Li, H. Cheng, Chem. Commun. 51 (2015) 3667–3670.
[135] Y. Yamada, A. Yamada, J. Electrochem. Soc. 162 (2015) A2406–A2423.
[136] J.T. Lee, H. Kim, M. Oschatz, D.C. Lee, F. Wu, H.T. Lin, B. Zdyrko, W.I. Cho, S. Kaskel, G. Yushin,Adv. Energy Mater. 5 (2015), 1400981.
[137] A. Hayashi, R. Ohtsubo, T. Ohtomo, F. Mizuno, M. Tatsumisago, J. Power Sources 183 (2008) 422–426.
[138] P.H.L. Notten, F. Roozeboom, R.A.H. Niessen, L. Baggetto, Adv. Mater. 19 (2007) 4564–4567.
[139] A. Sakuda, A. Hayashi, M. Tatsumisago, Sci. Rep. 3 (2013) 2261.
[140] X. Li, J. Liang, X. Li, C. Wang, J. Luo, R. Li, X. Sun, Energy Environ. Sci. 11 (2018) 2828–2832.
[141] M. Tatsumisago, M. Nagao, A. Hayashi, J. Am. Ceram. Soc. 1 (2018) 17–25.
[142] Q. Pan, D.M. Smith, H. Qi, S. Wang, C.Y. Li, Adv. Mater. 27 (2015) 5995–6001.
[143] Q. Wang, J. Jin, X. Wu, G. Ma, J. Yang, Z. Wen, Phys. Chem. Chem. Phys. 16 (2014) 21225–21229.
[144] P.V. Wright, MRS Bull. 27 (2011) 597–602.
[145] C. Wang, Q. Sun, Y. Liu, Y. Zhao, X. Lia, X. Lin, M.N. Banis, M. Li, W. Li, K.R. Adair, D. Wang, J. Liang, R. Li, L. Zhang, R. Yang, S. Lu, X. Sun, Nano Energy 48 (2018) 35–43.
[146] Y. Zhou, Z. Li, Y. Lu, Nano Energy 39 (2017) 554–561.
[147] F. Wu, J.T. Lee, N. Nitta, H. Kim, O. Borodin, G. Yushin, Adv. Mater. 27 (2015) 101–108.
[148] S.S. Zhang, J. Power Sources 162 (2006) 1379–1394.
[149] F.Cd. Godoi, D.W. Wang, Q. Zeng, K.H. Wu, I.R. Gentle, J. Power Sources 288 (2015) 13–19.
[150] A. Rosenman, R. Elazari, G. Salitra, E. Markevich, D. Aurbach, A. Garsuch, J. Electrochem. Soc. 162 (2015) A470–A473.
[151] S.S. Zhang, Electrochim. Acta 70 (2012) 344–348.
[152] J.Q. Huang, Z.L. Xu, S. Abouali, M. Akbari Garakani, J.K. Kim, Carbon 99 (2016) 624–632.
[153] L.-B. Xing, K. Xi, Q. Li, Z. Su, C. Lai, X. Zhao, R.V. Kumar, J. Power Sources 303 (2016) 22–28.
[154] L. Xu, S. Tang, Y. Cheng, K. Wang, J. Liang, C. Liu, Y.C. Cao, F. Wei, L. Mai, Joule 2 (2018) 1991–2015.
[155] C. Zu, Y.S. Su, Y. Fu, A. Manthiram, Phys. Chem. Chem. Phys. 15 (2013) 2291–2297.
[156] E.C. Cengiz, O. Ozturk, S.H. Soytas, R. Demir-Cakan, J. Power Sources 412 (2019) 472–479.
[157] X. Gu, C.J. Tong, S. Rehman, L.M. Liu, Y. Hou, S. Zhang, ACS Appl. Mater. Int. 8 (2016) 15991–16001.
[158] J. Li, Y. Yuan, H. Jin, H. Lu, A. Liu, D. Yin, J. Wang, J. Lu, S. Wang, Energy Storage Mater. 16 (2019) 31–36.

**Huan Du** is currently an undergraduate student from the International School of Materials Science and Engineering (ISMSE) at Wuhan University of Technology (WUT) since 2016. He has joined the tutorial system of undergraduates at the WUT Nano Key Laboratory and studies in Mai Research Group. His research interests involves nanomaterials and devices for energy storage.

**Wen Luo** received her Ph.D. degree in 2018 from the School of Materials Science and Engineering at Wuhan University of Technology under the supervision of Prof. Liqiang Mai. She was a visiting graduate student (2016–2017) in Prof. Jean-Jacques Gaumet Research Group at Université de Lorraine, France. She is currently an assistant professor at the Department of Physics, School of Science, Wuhan University of Technology. Her research focuses on nanomaterials and devices for energy storage and conversion.

**Liqiang Mai** is Chang Jiang Scholar Professor and Chair Professor of Materials Science and Engineering at Wuhan University of Technology (WUT). He is the winner of the National Natural Science Fund for Distinguished Young Scholars and Fellow of the Royal Society of Chemistry. He received his Ph.D. degree from WUT in 2004. He carried out his postdoctoral research in Prof. Zhonglin Wang's group at Georgia Institute of Technology in 2006–2007. He worked as advanced research scholar in the laboratory of Prof. Charles M. Lieber at Harvard University in 2008–2011 and the laboratory of Prof. Peidong Yang at University of California, Berkeley in 2017. His current research interests focus on new nanomaterials for electrochemical energy storage and micro/nano energy devices.

Please cite this article in press as: H. Du, et al., J. Mater. Sci. Technol. (2020), https://doi.org/10.1016/j.jmst.2020.01.001